Tensor-Based 2-D DOA Estimation for Uniform Planar Arrays With Unknown Mutual Coupling

Lei Yao, Ruoyu Zhang, *Senior Member, IEEE*, Changcheng Hu, Chengzhi Ye, *Student Member, IEEE*, Wen Wu, *Senior Member, IEEE*, and Byonghyo Shim, *Fellow, IEEE*

***Abstract*—For 2-D direction-of-arrival (2-D DOA) estimation, the uniform planar arrays (UPAs) can offer satisfactory estimation performance among various sensor array configurations, but are prone to being affected by the unknown mutual coupling effects. Existing 2-D DOA estimation algorithms accounting for the mutual coupling effects calibration either suffer from low estimation resolution or high computational complexity. To deal with this problem, we propose a tensor-based 2-D DOA estimation algorithm for UPAs in the presence of unknown mutual coupling. Specifically, by exploiting the block-banded symmetric Toeplitz structure of the mutual coupling matrix (MCM), we construct a calibration matrix to relieve the mutual coupling effect. Then, the received signals are reformulated into a tensor format admitting the canonical polyadic decomposition, where the factor matrices incorporate the azimuth and elevation angles. By exploiting the inherent Vandermonde structure of the equivalent steering matrix, we develop an algebraic-based factor matrix estimation method without the necessity of iteration, followed by the azimuth and elevation angles extraction from the estimated factor matrices. In addition, the closed-form solutions of the mutual coupling coefficients are obtained based on the estimated angles. On this basis, we mathematically investigate the uniqueness condition of the tensor decomposition and the maximum number of resolvable targets. Moreover, we derive the Cramér–Rao bound (CRB) to evaluate the performance limit for the considered 2-D DOA estimation problem with mutual coupling effects, and the computational complexity. Simulation results corroborate the superiority of the proposed tensor-based 2-D DOA estimation algorithm over competing methods in terms of complexity and resolution.**

***Index Terms*—2-D direction-of-arrival (DOA) estimation, mutual coupling calibration, tensor decomposition, uniform planar arrays (UPAs), Vandermonde structure.**

Received 10 November 2025; accepted 19 November 2025. Date of publication 1 December 2025; date of current version 26 January 2026. This work was supported in part by the National Natural Science Foundation of China under Grant 62571248 and Grant 62201266; in part by the Undergraduate Research Training Program of Nanjing University of Science and Technology under Grant 202510288068; and in part by the Ministry of Science and ICT (MSIT), South Korea, through the ITRC Support Program [supervised by Institute of Information and Communications Technology Planning and Evaluation (IITP)] under Grant IITP-2023-2021-0-02048. *(Corresponding author: Ruoyu Zhang.)*

Lei Yao and Chengzhi Ye are with the Key Laboratory of Near-Range RF Sensing ICs and Microsystems (NJUST), Ministry of Education, School of Electronic and Optical Engineering, and Qian Xuesen College, Nanjing University of Science and Technology, Nanjing 210094, China (e-mail: yaolei@njust.edu.cn; qxsycz8166@njust.edu.cn).

Ruoyu Zhang, Changcheng Hu, and Wen Wu are with the Key Laboratory of Near-Range RF Sensing ICs and Microsystems (NJUST), Ministry of Education, School of Electronic and Optical Engineering, Nanjing University of Science and Technology, Nanjing 210094, China (e-mail: ryzhang19@njust.edu.cn; huchangcheng@njust.edu.cn; wuwen@njust.edu.cn).

Byonghyo Shim is with the Department of Electrical and Computer Engineering and the Institute of New Media and Communications, Seoul National University, Seoul 08826, South Korea (e-mail: bshim@snu.ac.kr).

Digital Object Identifier 10.1109/JIOT.2025.3638991

I. Introduction

DIRECTION-OF-ARRIVAL (DOA) estimation is one of the most important problems in the field of array signal processing, having various applications such as wireless communications, radar, navigation, and the Internet of Things [1], [2], [3], [4]. Yet, to improve the estimation accuracy and resolution remains a significant challenge. Recently, an approach to employ the large-scale antenna arrays at the receiver end has emerged as a promising solution due to their ability to significantly enhance spatial resolution [5], [6], [7]. For example, when base stations are equipped with massive antenna arrays, massive multiple-input multiple-output (MIMO) technology can provide substantial improvements in spatial degrees of freedom [8], [9], [10]. Recently, metasurface-based antenna arrays, deployed in large planar structures, are popularly used in array signal processing, thereby promoting the importance of 2-D DOA estimation in wireless communication and sensing systems with uniform planar arrays (UPAs) [11], [12], [13].

Over the years, various DOA estimation techniques have been proposed to realize high-performance direction finding [14], [15], [16], [17], [18], [19], [20], [21]. Typically, to overcome the conventional beamforming method whose resolution is limited by the Rayleigh limit, a multiple signal classification (MUSIC) algorithm was developed via the exploitation of the orthogonality between the signal subspace and the noise subspace [14]. This algorithm broke through the Rayleigh limit and ushered in a new era of super-resolution algorithms. Despite its success in achieving higher performance, MUSIC requires computational complexity. Estimating signal parameters via the rotational invariance techniques (ESPRIT) algorithm utilized the rotational invariance of the array manifold to estimate the angles through eigenvalue decomposition and the properties of rotational invariant subspace [15]. This scheme strikes a relatively scalable trade-off between resolution and low computational complexity. With the rise of sparse representation [16] and compressed sensing theories [17], sparse reconstruction-based DOA estimation has been proposed. The essence of this approach is to transform the DOA estimation problem into a sparse signal reconstruction problem. Typical examples include ℓ_1-norm minimization [18] and orthogonal matching pursuit (OMP) [19]. Not coincidentally, researchers have also attempted to combine subspace decomposition with sparse representation to improve DOA estimation performance, leading to algorithms such as sparse Bayesian learning (SBL) [20].

One potential problem of these practical applications is that electromagnetic properties may lead to mutual coupling between array elements or sensors [22], causing interference between sensor responses. This phenomenon can adversely affect parameter estimation. One possible approach to mitigate mutual coupling effects is the use of sparse arrays, where the number of closely spaced sensor pairs is significantly less than that in a uniform linear array [23], [24]. State-of-the-art methods are in a bid to decouple or effectively eliminate mutual coupling effects from received data by employing appropriate models. In [25], a method capable of correcting for amplitude, phase, and mutual coupling effects without prior knowledge of correlations has been proposed. Another approach based on SBL has been presented in [26], which estimated the noise variance, mutual coupling vectors, and variance vectors of scattering coefficients via the expectation–maximization algorithm. Naturally, extending these algorithms to 2-D scenarios has also been a current research highlight. The study in [27] compensated for the effects by utilizing passive impedance elements, thereby fulfilling estimation objectives, and experimentally verified its effectiveness. A method based on UPAs was proposed in [28], considering this destructive phenomenon. By utilizing the MUSIC algorithm and selecting antennas at the edge as auxiliary receivers, this method achieved accurate estimation. In [29], the uniform circular array–rank reduction algorithm is combined with the root-MUSIC algorithm to achieve highly reliable estimation for uniform circular arrays.

The aforementioned approaches studied the collected, received data in the matrix format, overlooking the inherent connections embedded in the multidimensional structure of array data. When receiving data from 2-D or 3-D arrays, modeling the data based on the tensor signal processing is a promising option, and has emerged as a highly active research area [30], [31], [32], [33], [34], [35]. Xie et al. [36], [37], [38] introduced a higher-order tensor decomposition framework for joint 2-D direction-of-departure and DOA estimations in bistatic MIMO radar systems with UPAs, effectively preserving the inherent multidimensional structure of received signals and enabling automatic parameter pairing without additional alignment. In addressing the integrated communication and sensing problem with MIMO, an approach leveraging canonical polyadic tensor decomposition to construct both channel estimation and target parameter estimation using the same time–frequency resources has been proposed [39]. To better address the 2-D DOA estimation problem, a tensor decomposition-based multipath channel parameter estimation method capable of reconstructing wireless channels between any pair of mobile agents in the transmitting and receiving areas has been suggested [40]. In [41], a tensor-based technique has been proposed to estimate the angles of received signals from a 2-D cylindrical conformal antenna array. Also, a computationally efficient tensor decomposition method using an L-shaped array has been developed to independently estimate azimuth and elevation angles, achieving effective angle pairing through a spatial cross correlation matrix [42]. Based on the reconstructed tensor, Fu et al. [43] derived closed-form expressions for 2-D DOA and polarization parameters, avoiding the loss of array aperture and degrees of freedom, and achieving high-performance estimation. Although previous tensor-based methods can enhance parameter estimation performance to some extent, these approaches generally assume the ideal antenna array configurations, which, however, may suffer from significant performance degradation when there exist unknown mutual coupling effects in practice.

In this article, we address the 2-D DOA estimation problem for UPAs that are adversely affected by unknown mutual coupling by leveraging the tensor decomposition technique. The main contributions of this article are summarized as follows.

1) We establish a general model for the received signals affected by mutual coupling effects in the context of UPAs. By exploiting the block-banded symmetric Toeplitz structure of the mutual coupling matrix (MCM), we construct a calibration matrix to relieve the mutual coupling effects. Subsequently, the calibrated received signals are reformulated into a third-order canonical polyadic tensor format, such that the intrinsic multidimensional structure can be utilized.
2) We reframe the 2-D DOA estimation problem as the one to solve for factor matrices in the tensor decomposition. Instead of using the alternating least squares (ALS) method, we exploit the inherent Vandermonde structure of the equivalent steering vectors and develop an algebraic-based factor matrix estimation method. The azimuth and elevation angles, based on which the closed-form solutions of the mutual coupling coefficients are given, are then extracted from the estimated factor matrices.
3) We analyze the uniqueness condition of the tensor decomposition and the maximum number of resolvable targets, from which we validate the superiority of the proposed tensor-based 2-D DOA estimation algorithm. We also analyze the Cramér–Rao bound (CRB) for the considered 2-D DOA estimation problem with UPAs. The derived CRB can describe the best asymptotically achievable behavior of parameter estimation and evaluate the performance limit of our proposed algorithm. To more effectively elucidate the strengths of the tensor-based method exploiting the Vandermonde structure, we theoretically analyze its computational complexity.
4) We conduct numerical simulations to validate the superiority of the calibration method and the tensor-based 2-D DOA estimation algorithm. Meanwhile, there is a significant increase in the number of targets that could be estimated after leveraging the Vandermonde structure. When compared to existing approaches, the proposed tensor-based 2-D DOA estimation scheme exhibits lower complexity while maintaining high angle resolution, estimation accuracy, and mutual coupling coefficient correction performance.

Notations: Vectors and matrices are denoted by lowercase and uppercase boldface letters, respectively. $(\cdot)^{\mathrm{T}}$, $(\cdot)^{*}$, $(\cdot)^{\mathrm{H}}$, and $(\cdot)^{\dagger}$ represent the transpose, conjugate, conjugate transpose, and Moore–Penrose pseudoinverse operations, respectively. $\mathbf{I}_M$

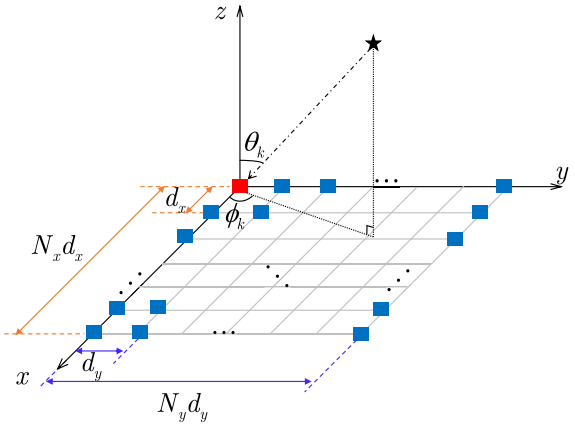

Fig. 1. Illustration of a 2-D DOA estimation model with UPAs.

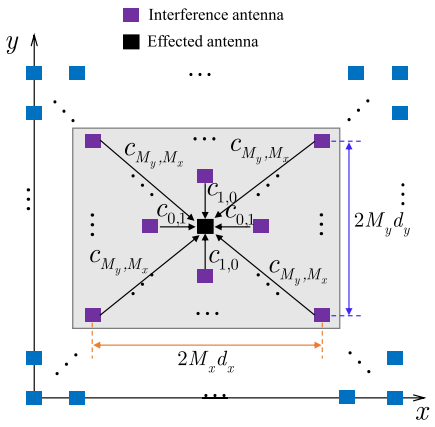

Fig. 2. Schematic of mutual coupling for UPAs.

is the $M \times M$ identity matrix and $\mathbf{0}_{M\times N}$ denotes a zero matrix with M rows and N columns. $j = \sqrt{-1}$ denotes an imaginary unit. $|\cdot|$, $\|\cdot\|_2$, and $\|\cdot\|_F$ denote the absolute value, ℓ_2 norm, and Frobenius norm, respectively. $\circledast$, $\odot$, $\otimes$, and $\circ$ denote the Hadamard product, Khatri–Rao product, Kronecker product, and outer product, respectively. The rank of $\mathbf{A}$ is denoted by rank($\mathbf{A}$). The symbol $\mathbb{E}\{\cdot\}$ denotes the expectation operation in probability theory. $\mathcal{R}\{\cdot\}$ extracts the real part of a complex number, while $\mathcal{CN}(0,\sigma^2)$ denotes the zero mean circularly symmetric complex Gaussian distribution with the variance of σ^2. $[\mathbf{a}]_m$ and $[\mathbf{A}]_{m,n}$ denote the mth entry and (m,n)th entry of $\mathbf{a}$ and $\mathbf{A}$, respectively. diag($\mathbf{A}$) denotes a vector formed by the diagonals of $\mathbf{A}$ and $\mathbf{A}^{(K_1,1)} = [\mathbf{A}^{(1)}]_{1:K_1,:}$ denotes the submatrix that extracts the first K_1 rows of $\mathbf{A}^{(1)}$. The symbols arcsin$(\cdot)$ and arctan$(\cdot)$ denote the inverse trigonometric functions of the sine and tangent functions, respectively. tr$\{\cdot\}$ denotes the trace of a matrix. The symbol toeplitz$\{\mathbf{c}\}$ denotes the symmetric Toeplitz matrix constructed by the vector $\mathbf{c}$. Given a vector $\mathbf{c} = [c_0, c_1, \ldots, c_{N-1}]^{\mathrm{T}}$ the Toeplitz matrix constructed from $\mathbf{c}$ is defined as follows:

$$\mathbf{T} = \text{toeplitz}(\mathbf{c}) = \begin{bmatrix} c_0 & c_1 & c_2 & \cdots & c_{N-1} \\ c_1 & c_0 & c_1 & \cdots & c_{N-2} \\ c_2 & c_1 & c_0 & \cdots & c_{N-3} \\ \vdots & \vdots & \vdots & \ddots & \vdots \\ c_{N-1} & c_{N-2} & c_{N-3} & \cdots & c_0 \end{bmatrix}. \tag{1}$$

II. Signal Model Formulation

As shown in Fig. 1, the UPA consists of N sensors, with a shape of N_x rows and N_y columns, such that $N = N_x N_y$. The interelement spacings along the x-axis and the y-axis for the array are denoted as d_x and d_y, respectively. Assuming that there are K far-field uncorrelated signals, with the kth incident signal from the direction (θ_k, ϕ_k), where θ_k and ϕ_k denote the elevation angle and the azimuth angle, respectively, $k = 1, 2, \ldots, K$. These far-field signals are assumed to have identical center wavelength λ, which is known to the receiver. By tradition, in the ideal condition without mutual coupling effect, we construct the received signal of the UPA at the tth snapshot, i.e., $\mathbf{x}(t) \in \mathbb{C}^{N\times 1}$, can be expressed as

$$\mathbf{x}(t) = \mathbf{A}\mathbf{s}(t) + \mathbf{n}(t) \tag{2}$$

where $\mathbf{s}(t) = [s_1(t), \ldots, s_K(t)]^{\mathrm{T}} \in \mathbb{C}^{K\times 1}$ is the source signal at the tth snapshot, $t = 1, 2, \ldots, T$, and $\mathbf{n}(t) \sim \mathcal{CN}(\mathbf{0}, \sigma_n^2 \mathbf{I}_N)$ are independent and identically distributed additive white Gaussian noise vectors with σ_n^2 being the noise power. Also, $\mathbf{A}$ is the steering matrix which is expressed as

$$\begin{aligned} \mathbf{A} &= \left[\mathbf{a}(\theta_1, \phi_1), \mathbf{a}(\theta_2, \phi_2), \ldots, \mathbf{a}(\theta_K, \phi_K)\right] \\ &= \mathbf{A}_y \odot \mathbf{A}_x \in \mathbb{C}^{N\times K} \end{aligned} \tag{3}$$

where $\mathbf{a}(\theta_k, \phi_k) = \mathbf{a}_y(\theta_k, \phi_k) \otimes \mathbf{a}_x(\theta_k, \phi_k) \in \mathbb{C}^{N\times 1}$, $\mathbf{A}_y \in \mathbb{C}^{N_y\times K}$, and $\mathbf{A}_x \in \mathbb{C}^{N_x\times K}$ are, respectively, expressed as

$$\mathbf{A}_y = \left[\mathbf{a}_y(\theta_1, \phi_1), \mathbf{a}_y(\theta_2, \phi_2), \ldots, \mathbf{a}_y(\theta_K, \phi_K)\right] \tag{4}$$

$$\mathbf{C} = \begin{bmatrix} \mathbf{C}_0 & \mathbf{C}_1 & \cdots & \mathbf{C}_{M_y} & \mathbf{0} & \cdots & \cdots & \cdots & \mathbf{0} \\ \mathbf{C}_1 & \mathbf{C}_0 & \mathbf{C}_1 & \cdots & \mathbf{C}_{M_y} & \mathbf{0} & \cdots & \cdots & \mathbf{0} \\ \vdots & \ddots & \ddots & \ddots & \ddots & \ddots & \ddots & \ddots & \vdots \\ \mathbf{C}_{M_y} & \cdots & \mathbf{C}_1 & \mathbf{C}_0 & \mathbf{C}_1 & \cdots & \mathbf{C}_{M_y} & \cdots & \mathbf{0} \\ \mathbf{0} & \ddots & \ddots & \ddots & \ddots & \ddots & \ddots & \ddots & \vdots \\ \vdots & \ddots & \mathbf{C}_{M_y} & \cdots & \mathbf{C}_1 & \mathbf{C}_0 & \mathbf{C}_1 & \cdots & \mathbf{C}_{M_y} \\ \vdots & \ddots & \ddots & \ddots & \ddots & \ddots & \ddots & \ddots & \vdots \\ \mathbf{0} & \cdots & \cdots & \mathbf{0} & \mathbf{C}_{M_y} & \cdots & \mathbf{C}_1 & \mathbf{C}_0 & \mathbf{C}_1 \\ \mathbf{0} & \cdots & \cdots & \cdots & \mathbf{0} & \mathbf{C}_{M_y} & \cdots & \mathbf{C}_1 & \mathbf{C}_0 \end{bmatrix} \tag{9}$$

$$\mathbf{A}_x = \left[\mathbf{a}_x(\theta_1,\phi_1), \mathbf{a}_x(\theta_2,\phi_2), \ldots, \mathbf{a}_x(\theta_K,\phi_K)\right] \tag{5}$$

where $\mathbf{a}_x(\theta_k,\phi_k)$ and $\mathbf{a}_y(\theta_k,\phi_k)$ are the steering vectors along the x- and y-axes, defined as

$$\mathbf{a}_x(\theta_k,\phi_k) = \left[1, \alpha_k, \ldots, \alpha_k^{N_x-1}\right]^{\mathrm{T}} \tag{6}$$

$$\mathbf{a}_y(\theta_k,\phi_k) = \left[1, \beta_k, \ldots, \beta_k^{N_y-1}\right]^{\mathrm{T}} \tag{7}$$

where $\alpha_k = e^{-j2\pi d_x v_k/\lambda}$ and $\beta_k = e^{-j2\pi d_y u_k/\lambda}$, defining parameters $u_k = \cos\phi_k \sin\theta_k$ and $v_k = \sin\phi_k \sin\theta_k$.

Fig. 2 depicts the mutual coupling phenomenon between adjacent antennas in UPAs, caused by electromagnetic field interactions [44]. Let M_x and M_y be the two constants describing the severity of mutual coupling along two orthogonal directions of UPAs, which means the mutual coupling effect exists not only between the array elements within each antenna subarray along the x-axis, but also between array elements among subarrays along the y-axis. Thus, the received signal $\mathbf{x}_c(t)$ accounting for mutual coupling effects can be expressed as

$$\mathbf{x}_c(t) = \mathbf{CAs}(t) + \mathbf{n}(t) \tag{8}$$

where $\mathbf{C} \in \mathbb{C}^{N\times N}$ denotes the MCM in UPAs and is given by (9), as shown at the bottom of the previous page.Specifically, $\mathbf{C}$ in (9) is in a block Toeplitz form, and each block $\mathbf{C}_{m_y} = \text{toeplitz}\{\tilde{\mathbf{c}}_{m_y}\} \in \mathbb{C}^{N_x\times N_x}$ represents a symmetric Toeplitz matrix constructed from the vector $\tilde{\mathbf{c}}_{m_y} = [\mathbf{c}_{m_y}^T, 0, \ldots, 0]^{\mathrm{T}} \in \mathbb{C}^{N_x\times 1}$, $\mathbf{c}_{m_y} = [c_{m_y,0}, c_{m_y,1}, \ldots, c_{m_y,M_x}]^{\mathrm{T}} \in \mathbb{C}^{(M_x+1)\times 1}$, and $m_y = 0, 1, \ldots, M_y$. Specifically, for the case $m_y = 0$, the first coefficient $c_{0,0} = 1$. According to (9), for an arbitrary given antenna element, it is hypothesized to experience mutual coupling effects from neighboring antennas within a surrounding $2M_x d_x \times 2M_y d_y$ rectangular region.

Subsequently, the covariance matrix $\mathbf{R}_c \in \mathbb{C}^{N\times N}$ of the received signals is

$$\mathbf{R}_c = \mathbb{E}\left\{\mathbf{x}_c(t)\mathbf{x}_c^H(t)\right\} = \mathbf{CAR}_s\mathbf{A}^H\mathbf{C}^H + \sigma_n^2\mathbf{I}_N \tag{10}$$

where $\mathbf{R}_s = \mathbb{E}\{\mathbf{s}(t)\mathbf{s}^H(t)\} \in \mathbb{C}^{K\times K}$ is the source covariance matrix. By the convention of the standard subspace approach, the covariance matrix of the received signal can be rewritten as

$$\mathbf{R}_c = \sum_{i=1}^{K}\lambda_i\mathbf{e}_i\mathbf{e}_i^H + \sum_{i=K+1}^{N}\lambda_i\mathbf{e}_i\mathbf{e}_i^H = \mathbf{E}_s\mathbf{\Lambda}_s\mathbf{E}_s^H + \sigma_n^2\mathbf{E}_n\mathbf{E}_n^H \tag{11}$$

where $\lambda_1 \geq \lambda_2 \geq \cdots \geq \lambda_K > \lambda_{K+1} = \cdots = \lambda_N$ are the eigenvalues of $\mathbf{R}_c$. $\mathbf{e}_1, \mathbf{e}_2, \ldots, \mathbf{e}_N$ are the eigenvectors associated with the K largest eigenvalues and $N-K$ smallest eigenvalues, respectively. Since the signal subspace is orthogonal to the noise subspace, we have

$$\mathbf{E}_n^H\mathbf{Ca}(\theta_k,\phi_k) = \mathbf{0} \quad \forall k = 1, 2, \ldots, K. \tag{12}$$

Under the influence of unknown mutual coupling effects, traditional subspace estimation methods will suffer from significant performance degradation due to the existence of $\mathbf{C}$. Existing estimation algorithms, such as the one in [28], suffer from a performance bottleneck and high computational complexity. To address this issue, in Section III, we will propose a tensor-based 2-D DOA and mutual coupling coefficients estimation algorithm for enhancing both accuracy and complexity performance.

III. Proposed Tensor-Based 2-D DOA and Mutual Coupling Coefficients Estimation Algorithm

In this section, we present a tensor-based technique, transforming the 2-D DOA estimation problem into tensor factorization. The essence of our approach is to exploit the Vandermonde structure to improve the maximum number of resolvable targets. We will also estimate the mutual coupling coefficients based on the angles obtained previously.

A. Calibration of Mutual Coupling Effects

Due to the fact that the presence of matrix $\mathbf{C}$ severely disrupts the original manifold array structure, conventional approaches might not be effective. In this work, we introduce the mutual coupling calibration to maintain the original model structure even when the mutual coupling effect exists.

For convenience, let $\widetilde{N}_x = N_x - 2M_x$ and $\widetilde{N}_y = N_y - 2M_y$. In order to calibrate the impact of mutual coupling effects from surrounding antennas, we introduce a block transformation matrix $\mathbf{T} \in \mathbb{C}^{\widetilde{N}_x\widetilde{N}_y\times N}$, whose form is given by

$$\mathbf{T} \triangleq \underbrace{\left[\begin{array}{ccc|ccc|ccc} \mathbf{T}_0 & \cdots & \mathbf{T}_0 & \widetilde{\mathbf{T}} & \cdots & \mathbf{T}_0 & \mathbf{T}_0 & \cdots & \mathbf{T}_0 \\ \vdots & \ddots & \vdots & \vdots & \ddots & \vdots & \vdots & \ddots & \vdots \\ \mathbf{T}_0 & \cdots & \mathbf{T}_0 & \mathbf{T}_0 & \cdots & \widetilde{\mathbf{T}} & \mathbf{T}_0 & \cdots & \mathbf{T}_0 \end{array}\right]}_{\text{zero matrix} \quad |\text{block diagonal matrix}| \quad \text{zero matrix}} \tag{13}$$

where $\mathbf{T}_0 = \mathbf{0}_{\widetilde{N}_x\times N_x}$ and $\widetilde{\mathbf{T}} = [\mathbf{0}_{\widetilde{N}_x\times M_x}\mathbf{I}_{\widetilde{N}_x}\mathbf{0}_{\widetilde{N}_x\times M_x}] \in \mathbb{C}^{\widetilde{N}_x\widetilde{N}_y\times N_x\widetilde{N}_y}$. The specific explanation for the block transformation matrix $\mathbf{T}$ is as follows. The left and right sides of this block matrix are composed of $\widetilde{N}_y \times M_y$ ($\widetilde{N}_y$ in row and M_y in column) zero matrices $\mathbf{T}_0$, respectively. For the middle part, there are a total of $\widetilde{N}_y \times \widetilde{N}_y$ submatrices, with the diagonal submatrices being $\widetilde{\mathbf{T}}$ and the remaining being zero matrices.

With the aid of the block transformation matrix $\mathbf{T}$, we present the following lemma [28].

Lemma 1: Based on the block transformation matrix $\mathbf{T}$, for the kth steering vector $\mathbf{a}(\theta_k,\phi_k)$ that is affected by the MCM $\mathbf{C}$, the following equality always holds true:

$$\mathbf{TCa}(\theta_k,\phi_k) = g_k\mathbf{Ta}(\theta_k,\phi_k) \tag{14}$$

where $g_k = \sum_{m_x=-M_x}^{M_x}\sum_{m_y=-M_y}^{M_y} c_{|m_y|,|m_x|}\alpha_k^{m_x}\beta_k^{m_y}$.

Proof: See Appendix A.□

Lemma 1 addresses this issue by employing a block transformation matrix $\mathbf{T}$, which converts the structural distortion caused by the MCM $\mathbf{C}$ into a complex-valued amplitude gain constant. It can also be deemed as a selection of the middle subarray, which is not arbitrary but mathematically optimal. In contrast, selecting boundary elements would introduce asymmetric coupling effects, resulting in a more complex mathematical structure that would degrade the accuracy of estimation. This transformation effectively eliminates the impact of the mutual coupling effects on the 2-D DOA estimation, while maintaining the inherent structural characteristics of the steering matrix $\mathbf{A}$.

B. Tensor Reformulation and Decomposition

In this section, we reformulate the received signal into a third-order tensor, transforming the 2-D DOA estimation problem into the solution for factor matrices. By exploiting the Vandermonde structure, we obtain a novel tensor decomposition method that does not require iteration in obtaining the desired factor matrices.

Based on the signal model in (8), we can express the reception matrix $\mathbf{X}_c = [\mathbf{x}_c(1), \mathbf{x}_c(2), \ldots, \mathbf{x}_c(T)] \in \mathbb{C}^{N\times T}$ with multiple snapshots as

$$\mathbf{X}_c = \mathbf{CAS} + \mathbf{N} \tag{15}$$

where $\mathbf{S} = [\mathbf{s}(1), \mathbf{s}(2), \ldots, \mathbf{s}(T)] \in \mathbb{C}^{K\times T}$ and $\mathbf{N} = [\mathbf{n}(1), \mathbf{n}(2), \ldots, \mathbf{n}(T)] \in \mathbb{C}^{N\times T}$. With Lemma 1, we obtain the calibrated signal matrix $\mathbf{Y} \in \mathbb{C}^{\widetilde{N}_x\widetilde{N}_y\times T}$, which is expressed as

$$\begin{aligned}\mathbf{Y} &= \mathbf{TX}_c \\ &= \mathbf{TAGS} + \widetilde{\mathbf{N}} \\ &= \left(\mathbf{T}_y\mathbf{A}_y \odot \mathbf{T}_x\mathbf{A}_x\right)\mathbf{GS} + \widetilde{\mathbf{N}}\end{aligned} \tag{16}$$

where $\widetilde{\mathbf{N}} = \mathbf{TN} \in \mathbb{C}^{\widetilde{N}_x\widetilde{N}_y\times T}$ *and* $\mathrm{diag}\{\mathbf{G}\} = [g_1, \ldots, g_K]^{\mathrm{T}} \in \mathbb{C}^{K\times 1}$. For the second equality in (16), it can be viewed as an extension of Lemma 1 to K targets. The third equality in (16) holds true owing to the key observation $\mathbf{T} = \mathbf{T}_y \otimes \mathbf{T}_x$, the property $(\mathbf{A}_1 \otimes \mathbf{A}_2)(\mathbf{A}_3 \odot \mathbf{A}_4) = (\mathbf{A}_1\mathbf{A}_3) \odot (\mathbf{A}_2\mathbf{A}_4)$, and the definition of

$$\mathbf{T}_x \triangleq \left[\mathbf{0}_{\widetilde{N}_x\times M_x}\mathbf{I}_{\widetilde{N}_x}\mathbf{0}_{\widetilde{N}_x\times M_x}\right] \in \mathbb{C}^{\widetilde{N}_x\times N_x} \tag{17}$$

$$\mathbf{T}_y \triangleq \left[\mathbf{0}_{\widetilde{N}_y\times M_y}\mathbf{I}_{\widetilde{N}_y}\mathbf{0}_{\widetilde{N}_y\times M_y}\right] \in \mathbb{C}^{\widetilde{N}_y\times N_y}. \tag{18}$$

Based on the theory of tensor decomposition [31], $\mathbf{Y}$ can be viewed as mode unfolding of a third-order tensor $\boldsymbol{\mathcal{Y}} \in \mathbb{C}^{\widetilde{N}_x\times\widetilde{N}_y\times T}$, with its (n_x, n_y, t)th entry being the $((n_y-1)\widetilde{N}_x + n_x)$th row and the tth column entry of $\mathbf{Y}$. Let $\mathbf{A}^{(1)}$, $\mathbf{A}^{(2)}$, and $\mathbf{A}^{(3)}$ be the factor matrices of $\boldsymbol{\mathcal{Y}}$, which admits the following CPD format:

$$\boldsymbol{\mathcal{Y}} = \sum_{k=1}^{K}\mathbf{a}_k^{(1)} \circ \mathbf{a}_k^{(2)} \circ \mathbf{a}_k^{(3)} + \boldsymbol{\mathcal{N}} \tag{19}$$

where $\mathbf{a}_k^{(1)}$, $\mathbf{a}_k^{(2)}$, and $\mathbf{a}_k^{(3)}$ are the kth columns of $\mathbf{A}^{(1)}$, $\mathbf{A}^{(2)}$, and $\mathbf{A}^{(3)}$, respectively, and $\boldsymbol{\mathcal{N}} \in \mathbb{C}^{\widetilde{N}_x\times\widetilde{N}_y\times T}$ is the noise term. The $(\tilde{n}_x, \tilde{n}_y, t)$th entry of $\boldsymbol{\mathcal{N}}$ is the $((\tilde{n}_y-1)\widetilde{N}_x + \tilde{n}_x)$th row and the tth column entry of $\widetilde{\mathbf{N}}$. Accordingly, (16) can be rewritten as

$$\mathbf{Y}_{(3)}^T = \left(\mathbf{A}^{(2)} \odot \mathbf{A}^{(1)}\right)\mathbf{A}^{(3)T} + \widetilde{\mathbf{N}} \tag{20}$$

where $\mathbf{Y}_{(3)} = \mathbf{Y}^T \in \mathbb{C}^{T\times\widetilde{N}_x\widetilde{N}_y}$ is the mode-3 unfolding of $\boldsymbol{\mathcal{Y}}$, $\mathbf{A}^{(2)} = \mathbf{T}_y\mathbf{A}_y \in \mathbb{C}^{\widetilde{N}_y\times K}$, $\mathbf{A}^{(1)} = \mathbf{T}_x\mathbf{A}_x \in \mathbb{C}^{\widetilde{N}_x\times K}$, and $\mathbf{A}^{(3)} = \mathbf{S}^T\mathbf{G}^T \in \mathbb{C}^{T\times K}$. Note that our goal is to estimate the unknown 2-D DOA parameters $\{\theta_k, \phi_k\}_{k=1}^K$ and thus the target parameter estimation problem can be formulated as

$$\min_{\{\theta_k,\phi_k\}_{k=1}^K}\left\|\boldsymbol{\mathcal{Y}} - \sum_{k=1}^{K}\mathbf{a}_k^{(1)} \circ \mathbf{a}_k^{(2)} \circ \mathbf{a}_k^{(3)}\right\|_F^2. \tag{21}$$

Thus, an effective strategy for the parameter estimation is to exploit the factor matrices of (19), which means the desired angle information can be obtained from CPD. A well-known technique is the ALS algorithm [40], where the iterative optimization is performed by systematically updating one factor matrix at a time while fixing the rest parameters. The procedure progresses through successive iterations, each cycle refining the factor matrices in a coordinated manner, until the solution converges to a stable state that satisfies the convergence criteria. Specifically, implementing the ALS algorithm to $\boldsymbol{\mathcal{Y}}$ in our model, we have

$$\mathbf{A}_{(i+1)}^{(1)} = \arg\min_{\mathbf{A}^{(1)}}\left\|\mathbf{Y}_{(1)} - \mathbf{A}^{(1)}\left(\mathbf{A}_{(i)}^{(3)} \odot \mathbf{A}_{(i)}^{(2)}\right)^{\mathrm{T}}\right\|_F^2 \tag{22}$$

$$\mathbf{A}_{(i+1)}^{(2)} = \arg\min_{\mathbf{A}^{(2)}}\left\|\mathbf{Y}_{(2)} - \mathbf{A}^{(2)}\left(\mathbf{A}_{(i)}^{(3)} \odot \mathbf{A}_{(i+1)}^{(1)}\right)^{\mathrm{T}}\right\|_F^2 \tag{23}$$

$$\mathbf{A}_{(i+1)}^{(3)} = \arg\min_{\mathbf{A}^{(3)}}\left\|\mathbf{Y}_{(3)} - \mathbf{A}^{(3)}\left(\mathbf{A}_{(i+1)}^{(2)} \odot \mathbf{A}_{(i+1)}^{(1)}\right)^{\mathrm{T}}\right\|_F^2 \tag{24}$$

where $\mathbf{Y}_{(1)}$ and $\mathbf{Y}_{(2)}$ take the matrix unfolding of $\boldsymbol{\mathcal{Y}}$ along its first and second dimension, while $\mathbf{A}_{(i)}^{(1)}$, $\mathbf{A}_{(i)}^{(2)}$, and $\mathbf{A}_{(i)}^{(3)}$ are the updated factor matrices at the ith iteration. Through iterative alternated execution of the three update procedures, the algorithm progressively refines the factor matrices until the suitably designed convergence criterion is satisfied, yielding the optimal estimates for the factor matrices denoted as $\{\hat{\mathbf{A}}^{(1)}, \hat{\mathbf{A}}^{(2)}, \hat{\mathbf{A}}^{(3)}\}$.

In (21), we find that $\mathbf{a}_k^{(2)}$ is a part of a steering vector, maintaining the power series structure. Thus, the factor matrix $\mathbf{A}^{(2)}$ exhibits a Vandermonde structure, with generators $\{z_{\beta,k} = e^{-j2\pi d_y u_k/\lambda}\}_{k=1}^K$. On this basis, we take into account the structural constraints of factor matrices and propose an algebraic-based factor matrix estimation method, which may avoid the necessity of iteration and even enhance the angle resolution for a larger number of targets. Specifically, we construct a cyclic selection matrix $\mathbf{J}_{l_2} = [\mathbf{0}_{K_2\times(l_2-1)}\ \mathbf{I}_{K_2}\ \mathbf{0}_{K_2\times(L_2-l_2)}] \otimes \mathbf{I}_{\widetilde{N}_x} \in \mathbb{C}^{K_2\widetilde{N}_x\times\widetilde{N}_y\widetilde{N}_x}$ and vary l_2 from 1 to L_2, yielding

$$\begin{aligned}\mathbf{Y}_S &= \left[\mathbf{J}_1\mathbf{Y}_{(3)}^T\ \mathbf{J}_2\mathbf{Y}_{(3)}^T, \ldots,\ \mathbf{J}_{L_2}\mathbf{Y}_{(3)}^T\right] \\ &= \left[\left(\mathbf{J}_1\mathbf{A}^{(2)}\right) \odot \mathbf{A}^{(1)}, \ldots, \left(\mathbf{J}_{L_2}\mathbf{A}^{(2)}\right) \odot \mathbf{A}^{(1)}\right] \\ &\quad \times \left(\mathbf{I}_{L_2} \otimes \mathbf{A}^{(3)}\right)^{\mathrm{T}} + \mathbf{N}_S \\ &= \left(\mathbf{A}^{(K_2,2)} \odot \mathbf{A}^{(1)}\right)\mathbf{\Lambda}^{-1} \\ &\quad \times \left[\mathbf{\Lambda}^1, \ldots, \mathbf{\Lambda}^{L_2}\right]\left(\mathbf{I}_{L_2} \otimes \mathbf{A}^{(3)}\right)^{\mathrm{T}} + \mathbf{N}_S \\ &= \left(\mathbf{A}^{(K_2,2)} \odot \mathbf{A}^{(1)}\right)\mathbf{\Lambda}^{-1} \\ &\quad \times \left(\left[\mathrm{diag}\left(\mathbf{\Lambda}^1\right), \ldots, \mathrm{diag}\left(\mathbf{\Lambda}^{L_2}\right)\right]^{\mathrm{T}} \odot \mathbf{A}^{(3)}\right)^{\mathrm{T}} + \mathbf{N}_S \\ &= \left(\mathbf{A}^{(K_2,2)} \odot \mathbf{A}^{(1)}\right)\mathbf{\Lambda}^{-1}\left(\mathbf{A}^{(L_2,2)} \odot \mathbf{A}^{(3)}\right)^{\mathrm{T}} + \mathbf{N}_S\end{aligned} \tag{25}$$

where $K_2 + L_2 = \widetilde{N}_y + 1$, $\mathbf{\Lambda}$ is a diagonal matrix, $\mathrm{diag}\{\mathbf{\Lambda}\} = [z_{\beta,1}^{M_x}, \ldots, z_{\beta,K}^{M_x}]^{\mathrm{T}} \in \mathbb{C}^{K\times 1}$, and $\mathbf{N}_S \in \mathbb{C}^{K_2\widetilde{N}_x\times L_2T}$ is the corresponding noise term. The second equality is guaranteed by exploiting the property $(\mathbf{A}_1 \otimes \mathbf{A}_2)(\mathbf{A}_3 \odot \mathbf{A}_4) = (\mathbf{A}_1\mathbf{A}_3) \odot (\mathbf{A}_2\mathbf{A}_4)$ and the third equality holds due to $z_{\beta,k}^{\widetilde{N}_y} = z_{\beta,k}^{K_2+L_2-1}$. For the fourth equality, it follows the fact that $\mathbf{A}^{(3)}\mathbf{\Lambda}^{l_2} = \mathrm{diag}\{\mathbf{\Lambda}^{l_2}\} \odot \mathbf{A}^{(3)}$. The last equality follows from the fact that $[\mathrm{diag}\{\mathbf{\Lambda}^1\}, \ldots, \mathrm{diag}\{\mathbf{\Lambda}^{L_2}\}]^{\mathrm{T}}$ can be represented by $\mathbf{A}^{(L_2,2)}$. To perform the factor matrices estimation, we utilize the ESPRIT-like method [39], computing the singular value decomposition in the first step, i.e.,$\mathbf{Y}_S = \mathbf{U}\mathbf{\Sigma}\mathbf{V}^H = \mathbf{U}_s\mathbf{\Sigma}_s\mathbf{V}_s^H + \mathbf{U}_n\mathbf{\Sigma}_n\mathbf{V}_n^H$, where the K principal singular vectors in $\mathbf{U}$ and $\mathbf{V}$ span the signal

subspaces $\mathbf{U}_s$ and $\mathbf{V}_s$, respectively, and $\mathbf{\Sigma}_s$ is diagonal matrix formed by the K largest singular values. For further processing, we define $\mathbf{U}_1 = [\mathbf{U}_s]_{1:(K_2-1)\widetilde{N}_x,:}$ and $\mathbf{U}_2 = [\mathbf{U}_s]_{\widetilde{N}_x+1:K_2\widetilde{N}_x,:}$, and compute the eigenvalue decomposition as $\mathbf{U}_1^{\dagger}\mathbf{U}_2 = \mathbf{MZM}^{-1}$ [50]. Accordingly, the kth column of the factor matrix $\hat{\mathbf{A}}^{(2)}$ can be reconstructed as

$$\hat{\mathbf{a}}_k^{(2)} = \left[\hat{z}_{\beta,k}^{M_y}, \hat{z}_{\beta,k}^{M_y+1}, \ldots, \hat{z}_{\beta,k}^{N_y-M_y-1}\right]^{\mathrm{T}} \tag{26}$$

where $\hat{z}_{\beta,k} = [\mathbf{Z}]_{k,k}/|[\mathbf{Z}]_{k,k}|$ is the estimated generator. Subsequently, the other two factor matrices $\hat{\mathbf{A}}^{(1)} = [\hat{\mathbf{a}}_1^{(1)}, \ldots, \hat{\mathbf{a}}_K^{(1)}]$ and $\hat{\mathbf{A}}^{(3)} = [\hat{\mathbf{a}}_1^{(3)}, \ldots, \hat{\mathbf{a}}_K^{(3)}]$ can be estimated, whose kth columns can be obtained via

$$\hat{\mathbf{a}}_k^{(1)} = \left(\hat{\mathbf{a}}_k^{(K_2,2)H} \otimes \mathbf{I}_{\widetilde{N}_x}\right)\mathbf{U}_s\mathbf{m}_k \tag{27}$$

$$\hat{\mathbf{a}}_k^{(3)} = \left(\hat{\mathbf{a}}_k^{(L_2,2)H} \otimes \mathbf{I}_T\right)\mathbf{V}_s^*\mathbf{\Sigma}_s\mathbf{t}_k \tag{28}$$

respectively, where $\mathbf{m}_k$ is the kth column of $\mathbf{M}$ and $\mathbf{t}_k$ is the kth column of $(\mathbf{M}^{-1})^*$. Similar procedure is applicable for the Vandermonde structure of $\mathbf{A}^{(1)}$.[1]

It is worth noting that the factor matrices obtained through CPD may exhibit inherent biases and are subject to two distinct types of ambiguities: scalar ambiguity and column permutation ambiguity. For the estimated factor matrices $\{\hat{\mathbf{A}}^{(1)}, \hat{\mathbf{A}}^{(2)}, \hat{\mathbf{A}}^{(3)}\}$, they satisfy the following relationship:

$$\hat{\mathbf{A}}^{(1)} = \mathbf{A}^{(1)}\mathbf{\Pi}\mathbf{\Lambda}_1 + \mathbf{E}_1 \tag{29}$$

$$\hat{\mathbf{A}}^{(2)} = \mathbf{A}^{(2)}\mathbf{\Pi}\mathbf{\Lambda}_2 + \mathbf{E}_2 \tag{30}$$

$$\hat{\mathbf{A}}^{(3)} = \mathbf{A}^{(3)}\mathbf{\Pi}\mathbf{\Lambda}_3 + \mathbf{E}_3 \tag{31}$$

where $\mathbf{\Pi}$ denotes a permutation matrix, $\mathbf{\Lambda}_1$–$\mathbf{\Lambda}_3$ are the diagonal matrices, and $\mathbf{E}_1$–$\mathbf{E}_3$ denote the errors of tensor decomposition. It can be seen from (29)–(31) that the column permutation, denoted as $\mathbf{\Pi}$, is the same for all factor matrices and thus does not disrupt the pairing relation among the estimated and true factor matrices, allowing each unknown parameter to be extracted from the corresponding column vector of factor matrices. As for scaling ambiguity, it is common for each column of factor matrices, and thus, it does not affect the estimation of angle parameters, as shown in the next section.

C. Estimation of 2-D DOA

So far, we have transformed the 2-D DOA estimation problem into a factor matrix estimation problem, which facilitates the acquisition of angle information through a gridless approach. This method enables more precise angular estimation without conventional spatial discretization constraints. Thus, our task is to extract the elevation and azimuth angles from the aforementioned factor matrices. To be specific, for $\hat{\mathbf{A}}^{(1)}$, the kth column of which is $\hat{\mathbf{a}}_k^{(1)}$, we have

$$\hat{\mathbf{a}}_k^{(1)} = \delta_{1,k}\widetilde{\mathbf{a}}_x(v_k) + \mathbf{e}_{1,k} \tag{32}$$

[1]For $\mathcal{Y}$, both factor matrices $\mathbf{A}^{(1)}$ and $\mathbf{A}^{(2)}$ exhibit Vandermonde structure. Therefore, we can propose an algorithm similar to the method utilizing cyclic selection matrices mentioned above, thereby fully leveraging the structural characteristics of the factor matrices. We construct a cyclic selection matrix $\bar{\mathbf{J}}_{l_2,l_1} = \check{\mathbf{J}}_{l_2} \otimes \check{\mathbf{J}}_{l_1} \in \mathbb{C}^{K_2K_1\times\widetilde{N}_y\widetilde{N}_x}$, where $\check{\mathbf{J}}_{l_2} = [\mathbf{0}_{K_2\times(l_2-1)}\ \mathbf{I}_{K_2}\ \mathbf{0}_{K_2\times(\underline{L}_2-l_2)}]$, $\check{\mathbf{J}}_{l_1} = [\mathbf{0}_{K_1\times(l_1-1)}\ \mathbf{I}_{K_1}\ \mathbf{0}_{K_1\times(L_1-l_1)}]$, $K_2 + L_2 = \widetilde{N}_y + 1$, and $K_1 + L_1 = \widetilde{N}_x + 1$. It is worth noting that l_2 varies from 1 to L_2 and l_1 varies from 1 to L_1.

where $\delta_{1,k}$ is the kth diagonal entry of $\mathbf{\Lambda}_1$ and $\mathbf{e}_{1,k}$ is the kth column of $\mathbf{E}_1$. Note that $\widetilde{\mathbf{a}}_x(v_k) = [\alpha_k^{M_x}, \ldots, \alpha_k^{N_x-M_x-1}]^{\mathrm{T}}$ is the kth column of $\mathbf{A}^{(1)}$. Due to the Vandermonde structure of $\mathbf{A}^{(1)}$, we can further obtain $[\hat{\mathbf{a}}_k^{(1)}]_{2:\widetilde{N}_x} = \alpha_k[\hat{\mathbf{a}}_k^{(1)}]_{1:\widetilde{N}_x-1}$ in the noiseless case. Leveraging the bijective correspondence between variables α_k and v_k, the parameter v_k can be accurately estimated by extracting the phase component from the complex variable α_k, which is explicitly represented as

$$\hat{v}_k = -\frac{\lambda}{2\pi d_x}\angle\hat{\alpha}_k, \quad k = 1, \ldots, K \tag{33}$$

where $\angle$ denotes the operator of phase angle extraction and $\hat{\alpha}_k = [\hat{\mathbf{a}}_k^{(1)}]^{\dagger}_{2:\widetilde{N}_x}[\hat{\mathbf{a}}_k^{(1)}]_{1:\widetilde{N}_x-1}$ is the estimated generator. The procedure is similar to the estimation process of the estimate of $\hat{u}_k$. $\hat{\mathbf{a}}_k^{(2)}$, defined as the kth column of $\hat{\mathbf{A}}^{(2)}$, is expressed as

$$\hat{\mathbf{a}}_k^{(2)} = \delta_{2,k}\widetilde{\mathbf{a}}_y(u_k) + \mathbf{e}_{2,k} \tag{34}$$

where $\delta_{2,k}$ is the kth diagonal entry of $\mathbf{\Lambda}_2$, $\mathbf{e}_{2,k}$ is the kth column of $\mathbf{E}_2$, and $\widetilde{\mathbf{a}}_y(u_k) = [\beta_k^{M_y}, \ldots, \beta_k^{N_y-M_y-1}]^{\mathrm{T}}$ is the kth column of $\mathbf{A}^{(2)}$. The expression $\hat{\beta}_k = [\hat{\mathbf{a}}_k^{(2)}]^{\dagger}_{2:\widetilde{N}_y}[\hat{\mathbf{a}}_k^{(2)}]_{1:\widetilde{N}_y-1}$ can be derived because of the Vandermonde structure of $\mathbf{A}^{(2)}$, and $\hat{u}_k$ is computed by

$$\hat{u}_k = -\frac{\lambda}{2\pi d_y}\angle\hat{\beta}_k, \quad k = 1, \ldots, K. \tag{35}$$

Once u_k and v_k are computed, elevation and azimuth angles, θ_k and ϕ_k, can be derived through elementary trigonometric operations. The facts that $\hat{u}_k = \cos\hat{\phi}_k \sin\hat{\theta}_k$ and $\hat{v}_k = \sin\hat{\phi}_k \sin\hat{\theta}_k$ establish a bijective mapping between the input and output parameters

$$\hat{\theta}_k = \arcsin\left(\sqrt{\hat{u}_k^2 + \hat{v}_k^2}\right) \tag{36a}$$

$$\hat{\phi}_k = \arctan\left(\frac{\hat{v}_k}{\hat{u}_k}\right). \tag{36b}$$

D. Estimation of Mutual Coupling Coefficients

In this section, we discuss a mutual coupling coefficient estimation technique using the subspace decomposition. Before presenting the corresponding processing steps, we will first introduce a relevant lemma, reexpressing the unknown coupling coefficients in a structured and separable form.

Lemma 2: For any banded symmetric Toeplitz matrix $\mathbf{W} \in \mathbb{C}^{M\times M}$ and column vector $\mathbf{a} \in \mathbb{C}^{M\times 1}$, the following transformation holds:

$$\mathbf{Wa} = \mathbf{Q}(\mathbf{a})\,\mathbf{w} \tag{37}$$

where $\mathbf{w} \in \mathbb{C}^{P\times 1}$ with the ith element being $[\mathbf{w}]_i = [\mathbf{W}]_{1,i}$, $i = 1, 2, \ldots, P$. P is the number of nonzero elements in the first row of matrix $\mathbf{W}$. $\mathbf{Q}(\mathbf{a}) \in \mathbb{C}^{M\times P}$ is expressed as follows:

$$\mathbf{Q}(\mathbf{a}) = \mathbf{Q}_1(\mathbf{a}) + \mathbf{Q}_2(\mathbf{a}) \tag{38}$$

$$[\mathbf{Q}_1(\mathbf{a})]_{i,j} = \begin{cases}[\mathbf{a}]_{i+j-1}, & \text{if } i+j \le M+1\\ 0, & \text{otherwise}\end{cases} \tag{39}$$

$$[\mathbf{Q}_2(\mathbf{a})]_{i,j} = \begin{cases}[\mathbf{a}]_{i-j+1}, & \text{if } i \le j \le 2\\ 0, & \text{otherwise.}\end{cases} \tag{40}$$

Proof: This lemma can be directly verified through elementary matrix operations. A similar procedure appears in [47].□

Lemma 2 transforms a symmetric Toeplitz matrix to a corresponding vector for further processing. By applying Lemma 2 to the submatrix $\mathbf{C}_{m_y}$, we can obtain

$$\mathbf{C}_{m_y}\mathbf{a}_x(\theta_k,\phi_k) = \mathbf{Q}(\mathbf{a}_x(\theta_k,\phi_k))\,\mathbf{c}_{m_y} \tag{41}$$

where $\mathbf{c}_{m_y} = [c_{m_y,0},\ldots,c_{m_y,M_x}]^{\mathrm{T}} \in \mathbb{C}^{(M_x+1)\times 1}$. As a further step, we consider the whole MCM $\mathbf{C}$, then we have

$$\begin{aligned}\mathbf{C}\mathbf{a}(\theta_k,\phi_k) &= \mathbf{C}\left(\mathbf{a}_y(\theta_k,\phi_k)\otimes\mathbf{a}_x(\theta_k,\phi_k)\right)\\ &= \begin{bmatrix} \sum_{n_y=1}^{N_y}\left[\mathbf{a}_y\right]_{n_y}\mathbf{C}_{|n_y-1|}\mathbf{a}_x \\ \sum_{n_y=1}^{N_y}\left[\mathbf{a}_y\right]_{n_y}\mathbf{C}_{|n_y-2|}\mathbf{a}_x \\ \vdots \\ \sum_{n_y=1}^{N_y}\left[\mathbf{a}_y\right]_{n_y}\mathbf{C}_{|n_y-N_y|}\mathbf{a}_x \end{bmatrix}\\ &= \left[\mathbf{Q}_{y,k}\otimes\mathbf{Q}_{x,k}\right]\tilde{\mathbf{c}}\end{aligned} \tag{42}$$

where $\mathbf{Q}_{y,k} = \mathbf{Q}(\mathbf{a}_y(\theta_k,\phi_k)) \in \mathbb{C}^{N_y\times(M_y+1)}$ and $\mathbf{Q}_{x,k} = \mathbf{Q}(\mathbf{a}_x(\theta_k,\phi_k)) \in \mathbb{C}^{N_x\times(M_x+1)}$ share the same mathematical structure. The third equality of (42) is guaranteed by the facts that $\mathbf{C}_{m_y} = \mathbf{0}_{N_x\times N_x}, m_y = M_y+1,\ldots,N_y$, (41), and the definition $\tilde{\mathbf{c}} \triangleq [\mathbf{c}_0^T,\mathbf{c}_1^T,\ldots,\mathbf{c}_{M_y}^T]^{\mathrm{T}} \in \mathbb{C}^{(M_x+1)(M_y+1)\times 1}$.

It is noted that $\tilde{\mathbf{c}}$ encompasses all the unknown mutual coupling coefficients. Simultaneously, in (42), the array steering vector has only undergone rearrangement, involving all the array elements in the planar array. By substituting (42) into (12), we obtain

$$\mathbf{E}_n^H\left(\mathbf{Q}_{y,k}\otimes\mathbf{Q}_{x,k}\right)\tilde{\mathbf{c}} = \mathbf{0}. \tag{43}$$

By translating (43) into its scalar form

$$\tilde{\mathbf{c}}^H\left(\mathbf{Q}_{y,k}\otimes\mathbf{Q}_{x,k}\right)^H\mathbf{E}_n\mathbf{E}_n^H\left(\mathbf{Q}_{y,k}\otimes\mathbf{Q}_{x,k}\right)\tilde{\mathbf{c}} = 0. \tag{44}$$

It can be seen from (44) that the vector $\tilde{\mathbf{c}}$ is the eigenvector corresponding to the zero eigenvalue of the Hermitian matrix

$$\mathbf{\Gamma}(u_k,v_k) = \left(\mathbf{Q}_{y,k}\otimes\mathbf{Q}_{x,k}\right)^H\mathbf{E}_n\mathbf{E}_n^H\left(\mathbf{Q}_{y,k}\otimes\mathbf{Q}_{x,k}\right) \tag{45}$$

where $\mathbf{\Gamma}(u_k,v_k) \in \mathbb{C}^{(M_x+1)(M_y+1)\times(M_x+1)(M_y+1)}$. Under the rank deficiency condition, it can be proven that matrix $\mathbf{\Gamma}(u,v)$ is rank-one deficient [46], which implies that there is only one linearly independent eigenvector corresponding to its zero eigenvalue. Therefore, by utilizing all the estimated parameter sets $\{\hat{u}_k,\hat{v}_k\}_{k=1}^K$, we can construct the decoupling matrix $\mathbf{\Psi}$ as

$$\mathbf{\Psi} = \sum_{k=1}^{K}\mathbf{\Gamma}(\hat{u}_k,\hat{v}_k). \tag{46}$$

After performing eigenvalue decomposition on $\mathbf{\Psi}$ in (46), we can obtain the smallest eigenvalue of $\mathbf{\Psi}$, denoted as $\mathbf{e}_{\min}$. Since the first element of the mutual coupling vector $\tilde{\mathbf{c}}$ takes a value of 1, we need to normalize it, that is,

$$\hat{\tilde{\mathbf{c}}} = \mathbf{e}_{\min}/\mathbf{e}_{\min}(1) \tag{47}$$

Algorithm 1 Proposed Tensor-Based 2-D DOA and Mutual Coupling Coefficients Estimation Algorithm

Input: Received signals $\mathbf{X}_c$, array parameters N_x, N_y, M_x, M_y, d_x, d_y.

1: Compute calibration matrix $\mathbf{T}$ using (13);
2: Compute refined signal $\mathbf{Y}_{(3)}^T$ using (16);
3: Compute $\mathbf{Y}_S$ using (25);
4: Estimate factor matrices $\hat{\mathbf{A}}^{(1)}$, $\hat{\mathbf{A}}^{(2)}$, and $\hat{\mathbf{A}}^{(3)}$ using (26)-(28);
5: Estimate parameter $\{\hat{u}_k,\hat{v}_k\}_{k=1}^K$ using (33) and (35);
6: Compute $\{\hat{\theta}_k,\hat{\phi}_k\}_{k=1}^K$ using (36);
7: Construct decoupling matrix $\mathbf{\Psi}$ using (46);
8: Perform eigenvalue decomposition on $\mathbf{\Psi}$;
9: Compute $\hat{\tilde{\mathbf{c}}}$ using (47);

Output: Estimated elevations and azimuths $\{\hat{\theta}_k,\hat{\phi}_k\}_{k=1}^K$ and mutual coupling coefficients $\hat{\tilde{\mathbf{c}}}$.

where $\mathbf{e}_{\min}(1)$ is the first element of $\mathbf{e}_{\min}$. Consequently, the mutual coupling coefficients can be unambiguously estimated, allowing for the reconstruction of the MCM.

To this end, the 2-D DOA of sources and the unknown mutual coupling coefficients can be obtained, which is summarized in Algorithm 1.

IV. Performance Analysis

A. Uniqueness Condition

The uniqueness of CPD provides the essential guarantee that the mathematically decomposed factors directly correspond to the angle information we seek to estimate. For a general case, it can be guaranteed by Kruskal's condition [45], which is given as follows.

Lemma 3: Let $\mathbf{A}^{(1)} \in \mathbb{C}^{I_1\times K}, \mathbf{A}^{(2)} \in \mathbb{C}^{I_2\times K}$, and $\mathbf{A}^{(3)} \in \mathbb{C}^{I_3\times K}$ be the factor matrices of a third-order tensor $\boldsymbol{\mathcal{X}} \in \mathbb{C}^{I_1\times I_2\times I_3}$ with rank K. If the following inequality holds:

$$\min(I_1,K)+\min(I_2,K)+\min(I_3,K) \geq 2K+2 \tag{48}$$

then, the CPD of $\boldsymbol{\mathcal{X}}$ is unique.

Proof: Refer to [45] for details.□

Lemma 3 offers a sufficient condition for establishing the uniqueness of the CPD problem. Alternatively, when the number of receive antennas is specified, the maximum number of targets K that can be recovered is determined. This recoverable limit for K can be further extended by leveraging the algebraic structures of the factor matrices, such as the Vandermonde structure. With such structural information, one can obtain the following relaxed uniqueness condition.

Lemma 4: Let $\mathbf{A}^{(1)} \in \mathbb{C}^{I_1\times K}$, $\mathbf{A}^{(2)} \in \mathbb{C}^{I_2\times K}$, and $\mathbf{A}^{(3)} \in \mathbb{C}^{I_3\times K}$ be the factor matrices of $\boldsymbol{\mathcal{X}} \in \mathbb{C}^{I_1\times I_2\times I_3}$, where $\mathbf{A}^{(2)}$ exhibits the Vandermonde structure. If

$$\begin{cases}\operatorname{rank}\left(\mathbf{A}^{(K_2-1,2)}\odot\mathbf{A}^{(1)}\right) = K\\ \operatorname{rank}\left(\mathbf{A}^{(L_2,2)}\odot\mathbf{A}^{(3)}\right) = K\end{cases} \tag{49}$$

with $K_2+L_2 = I_2+1$, the CPD of $\boldsymbol{\mathcal{X}}$ is said to be unique. In the generic case, (49) becomes

$$\min(I_1(K_2-1),I_3L_2) \geq K. \tag{50}$$

TABLE I
MAXIMUM NUMBER OF RESOLVABLE TARGETS UNDER THE UNIQUENESS CONDITIONS GIVEN IN LEMMAS 3 AND 4, WHERE $\widetilde{N}_y = 8$ AND $T = 100$

$\widetilde{N}_x$	8	10	12	14
Lemma 3	14	16	18	20
Lemma 4, $K_2 = 4$	24	30	36	42
Lemma 4, $K_2 = 6$	40	50	60	70
Lemma 4, $K_2 = 8$	56	70	84	98

Proof: Basically, the proof similarly follows the procedure in [51] by taking the mode-3 unfolding of $\mathcal{Y}$ in the noiseless setting, i.e., $\mathbf{Y}_{(3)}^T = (\mathbf{A}^{(2)} \odot \mathbf{A}^{(1)})\mathbf{A}^{(3)T}$.□

Lemma 4 introduces a strengthened identifiability guarantee for Vandermonde-structured CPD problems, with two key implications for parameter estimation in practical systems. First, unlike conventional CPD models, the uniqueness condition in Lemma 4 is maintained even when the factor matrices contain linearly dependent columns. Consequently, the spatial resolution for 2-D DOA estimation can be significantly improved. Second, Lemma 4 verifies that it is possible to deal with the CPD problem with a higher tensor rank than that of traditional CPD models without structural constraints. This relaxation of rank limitations directly translates to a higher upper bound on the number of resolvable targets, as the Vandermonde structure imposes exploitable algebraic regularities. To quantify this advancement, Table I contrasts the maximal number of sources K under different uniqueness conditions, demonstrating that Lemma 4 substantially broadens the feasible operational regime for high-resolution 2-D DOA estimation.

B. Analysis of CRB

CRB is utilized as a lower bound for the variance of unbiased estimators [3]. In our model, the real-valued unknown parameters are $\boldsymbol{\eta} = [\boldsymbol{\theta}^T, \boldsymbol{\phi}^T, \bar{\boldsymbol{\xi}}^T, \tilde{\boldsymbol{\xi}}^T]^{\mathrm{T}} \in \mathbb{C}^{(2K+2\widetilde{M})\times 1}$, where $\boldsymbol{\theta} = [\theta_1, \ldots, \theta_K]^{\mathrm{T}}$, $\boldsymbol{\phi} = [\phi_1, \ldots, \phi_K]^{\mathrm{T}}$, and $\widetilde{M} \triangleq M_x M_y + M_x + M_y$. $\bar{\boldsymbol{\xi}} \in \mathbb{C}^{\widetilde{M}\times 1}$ and $\tilde{\boldsymbol{\xi}} \in \mathbb{C}^{\widetilde{M}\times 1}$ are the real and imaginary parts of the elements in $\tilde{\mathbf{c}}$ except $c_{0,0}$, since in our model it is known and $c_{0,0} \equiv 1$. In [28], the case where $M_x = M_y = 1$, $c_{0,1} = c_{1,0}$ has been studied. While this is a specific case, our work extends the issue to a more general scenario. Hence, some similar derivations will be omitted, which can be found in [28]. For the mutual coupling-effected UPA, the general Fisher information matrix (FIM) is

$$[\mathbf{F}]_{m_i,m_j} = T\mathrm{tr}\left\{\mathbf{R}_c^{-1}\frac{\partial \mathbf{R}_c}{\partial \boldsymbol{\eta}_{m_i}}\mathbf{R}_c^{-1}\frac{\partial \mathbf{R}_c}{\partial \boldsymbol{\eta}_{m_j}}\right\} \tag{51}$$

where $m_i, m_j = 1, \ldots, 2K + 2\widetilde{M}$ and $\mathbf{R}_c$ denotes the covariance matrix of the received signals defined in (10). For the considered DOA estimation problem with unknown parameters $\boldsymbol{\eta}$, the FIM can be expressed as (52), as shown at the bottom of the page.To be specific, the top-left part of $\mathbf{F}$ is matrices, the top-right part is column vectors, the bottom-left part is row vectors, and the bottom-right part is composed of scalars. To obtain the concrete expression of the elements in $\mathbf{F}$, we need to define the following notations:

$$\dot{\mathbf{A}}_{\boldsymbol{\theta}} \triangleq \left[\mathbf{C}\frac{\partial \mathbf{a}(\theta_1,\phi_1)}{\partial \theta_1}, \ldots, \mathbf{C}\frac{\partial \mathbf{a}(\theta_K,\phi_K)}{\partial \theta_K}\right] \tag{53}$$

$$\dot{\mathbf{A}}_{\boldsymbol{\phi}} \triangleq \left[\mathbf{C}\frac{\partial \mathbf{a}(\theta_1,\phi_1)}{\partial \phi_1}, \ldots, \mathbf{C}\frac{\partial \mathbf{a}(\theta_K,\phi_K)}{\partial \phi_K}\right]. \tag{54}$$

The FIM consists four parts and the respective typical elements are

$$\mathbf{F}_{\boldsymbol{\theta\theta}} = 2T\mathcal{R}\left\{\left(\mathbf{R}_s\bar{\mathbf{A}}^H\mathbf{R}_c^{-1}\dot{\mathbf{A}}_{\boldsymbol{\theta}}\right)\circledast\left(\mathbf{R}_s\bar{\mathbf{A}}^H\mathbf{R}_c^{-1}\dot{\mathbf{A}}_{\boldsymbol{\theta}}\right)^{\mathrm{T}} + \left(\mathbf{R}_s\bar{\mathbf{A}}^H\mathbf{R}_c^{-1}\bar{\mathbf{A}}\mathbf{R}_s\right)\circledast\left(\dot{\mathbf{A}}_{\boldsymbol{\theta}}^H\mathbf{R}_c^{-1}\dot{\mathbf{A}}_{\boldsymbol{\theta}}\right)^{\mathrm{T}}\right\} \tag{55}$$

$$\mathbf{F}_{\boldsymbol{\phi\phi}} = 2T\mathcal{R}\left\{\left(\mathbf{R}_s\bar{\mathbf{A}}^H\mathbf{R}_c^{-1}\dot{\mathbf{A}}_{\boldsymbol{\phi}}\right)\circledast\left(\mathbf{R}_s\bar{\mathbf{A}}^H\mathbf{R}_c^{-1}\dot{\mathbf{A}}_{\boldsymbol{\phi}}\right)^{\mathrm{T}} + \left(\mathbf{R}_s\bar{\mathbf{A}}^H\mathbf{R}_c^{-1}\bar{\mathbf{A}}\mathbf{R}_s\right)\circledast\left(\dot{\mathbf{A}}_{\boldsymbol{\phi}}^H\mathbf{R}_c^{-1}\dot{\mathbf{A}}_{\boldsymbol{\phi}}\right)^{\mathrm{T}}\right\} \tag{56}$$

$$F_{\bar{\xi}_i\bar{\xi}_j} = 2T\mathcal{R}\left\{\mathrm{tr}\left\{\mathbf{R}_c^{-1}\dot{\bar{\mathbf{A}}}_{\bar{\xi}_i}\mathbf{R}_s\bar{\mathbf{A}}^H\mathbf{R}_c^{-1}\dot{\bar{\mathbf{A}}}_{\bar{\xi}_i}\mathbf{R}_s\bar{\mathbf{A}}^H\right\} + \mathrm{tr}\left\{\mathbf{R}_c^{-1}\dot{\bar{\mathbf{A}}}_{\bar{\xi}_i}\mathbf{R}_s\bar{\mathbf{A}}^H\mathbf{R}_c^{-1}\bar{\mathbf{A}}\mathbf{R}_s\dot{\bar{\mathbf{A}}}_{\bar{\xi}_i}^H\right\}\right\} \tag{57}$$

$$F_{\tilde{\xi}_i\tilde{\xi}_j} = 2T\mathcal{R}\left\{\mathrm{tr}\left\{\mathbf{R}_c^{-1}\dot{\tilde{\mathbf{A}}}_{\tilde{\xi}_i}\mathbf{R}_s\bar{\mathbf{A}}^H\mathbf{R}_c^{-1}\dot{\tilde{\mathbf{A}}}_{\tilde{\xi}_i}\mathbf{R}_s\bar{\mathbf{A}}^H\right\} + \mathrm{tr}\left\{\mathbf{R}_c^{-1}\dot{\tilde{\mathbf{A}}}_{\tilde{\xi}_i}\mathbf{R}_s\bar{\mathbf{A}}^H\mathbf{R}_c^{-1}\bar{\mathbf{A}}\mathbf{R}_s\dot{\tilde{\mathbf{A}}}_{\tilde{\xi}_i}^H\right\}\right\} \tag{58}$$

where $\bar{\xi}_i$ and $\tilde{\xi}_i$ denote the ith element of $\bar{\boldsymbol{\xi}}$ and $\tilde{\boldsymbol{\xi}}$, respectively, $\bar{\mathbf{A}} = \mathbf{CA}$, and $\dot{\bar{\mathbf{A}}}_{\bar{\xi}_i} = (\partial\mathbf{C})/(\partial\bar{\xi}_i)\mathbf{A}$, $\dot{\tilde{\mathbf{A}}}_{\tilde{\xi}_i} = (\partial\mathbf{C})/(\partial\tilde{\xi}_i)\mathbf{A}$. Due to the symmetry in structure of (51), we can derive the entire FIM, which is shown in (52). Some of the elements in (52) are given by (55)–(58). Please refer to Appendix B for detailed derivation. After obtaining the expression for all terms of $\mathbf{F}$,

$$\mathbf{F} = \left[\begin{array}{cc|ccccc} \mathbf{F}_{\boldsymbol{\theta\theta}} & \mathbf{F}_{\boldsymbol{\theta\phi}} & \mathbf{f}_{\boldsymbol{\theta}\bar{\xi}_1} & \cdots & \mathbf{f}_{\boldsymbol{\theta}\bar{\xi}_{\widetilde{M}}} & \mathbf{f}_{\boldsymbol{\theta}\tilde{\xi}_1} & \cdots & \mathbf{f}_{\boldsymbol{\theta}\tilde{\xi}_{\widetilde{M}}} \\ \mathbf{F}_{\boldsymbol{\phi\theta}} & \mathbf{F}_{\boldsymbol{\phi\phi}} & \mathbf{f}_{\boldsymbol{\phi}\bar{\xi}_1} & \cdots & \mathbf{f}_{\boldsymbol{\phi}\bar{\xi}_{\widetilde{M}}} & \mathbf{f}_{\boldsymbol{\phi}\tilde{\xi}_1} & \cdots & \mathbf{f}_{\boldsymbol{\phi}\tilde{\xi}_{\widetilde{M}}} \\ \mathbf{f}_{\boldsymbol{\theta}\bar{\xi}_1}^T & \mathbf{f}_{\boldsymbol{\phi}\bar{\xi}_1}^T & F_{\bar{\xi}_1\bar{\xi}_1} & \cdots & F_{\bar{\xi}_1\bar{\xi}_{\widetilde{M}}} & F_{\bar{\xi}_1\tilde{\xi}_1} & \cdots & F_{\bar{\xi}_1\tilde{\xi}_{\widetilde{M}}} \\ \vdots & \vdots & \vdots & \ddots & \vdots & \vdots & \ddots & \vdots \\ \mathbf{f}_{\boldsymbol{\theta}\bar{\xi}_{\widetilde{M}}}^T & \mathbf{f}_{\boldsymbol{\phi}\bar{\xi}_{\widetilde{M}}}^T & F_{\bar{\xi}_{\widetilde{M}}\bar{\xi}_1} & \cdots & F_{\bar{\xi}_{\widetilde{M}}\bar{\xi}_{\widetilde{M}}} & F_{\bar{\xi}_{\widetilde{M}}\tilde{\xi}_1} & \cdots & F_{\bar{\xi}_{\widetilde{M}}\tilde{\xi}_{\widetilde{M}}} \\ \mathbf{f}_{\boldsymbol{\theta}\tilde{\xi}_1}^T & \mathbf{f}_{\boldsymbol{\phi}\tilde{\xi}_1}^T & F_{\tilde{\xi}_1\bar{\xi}_1} & \cdots & F_{\tilde{\xi}_1\bar{\xi}_{\widetilde{M}}} & F_{\tilde{\xi}_1\tilde{\xi}_1} & \cdots & F_{\tilde{\xi}_1\tilde{\xi}_{\widetilde{M}}} \\ \vdots & \vdots & \vdots & \ddots & \vdots & \vdots & \ddots & \vdots \\ \mathbf{f}_{\boldsymbol{\theta}\tilde{\xi}_{\widetilde{M}}}^T & \mathbf{f}_{\boldsymbol{\phi}\tilde{\xi}_{\widetilde{M}}}^T & F_{\tilde{\xi}_{\widetilde{M}}\bar{\xi}_1} & \cdots & F_{\tilde{\xi}_{\widetilde{M}}\bar{\xi}_{\widetilde{M}}} & F_{\tilde{\xi}_{\widetilde{M}}\tilde{\xi}_1} & \cdots & F_{\tilde{\xi}_{\widetilde{M}}\tilde{\xi}_{\widetilde{M}}} \end{array}\right] \in \mathbb{C}^{(2K+2\widetilde{M})\times(2K+2\widetilde{M})} \tag{52}$$

we can derive the CRB for the unknown variable $\boldsymbol{\eta}$, i.e., $\mathbf{CRB}(\boldsymbol{\eta}) = \mathbf{F}^{-1}$, and

$$\mathrm{CRB}_1 = \sqrt{\frac{1}{2K}\sum_{\tilde{k}=1}^{2K}\left[\mathbf{CRB}\left(\boldsymbol{\eta}\right)\right]_{\tilde{k},\tilde{k}}} \tag{59}$$

$$\mathrm{CRB}_2 = \sqrt{\frac{1}{\|\tilde{\mathbf{c}}\|^2}\sum_{\tilde{m}=2K+1}^{2K+2\widetilde{M}}\left[\mathbf{CRB}\left(\boldsymbol{\eta}\right)\right]_{\tilde{m},\tilde{m}}} \tag{60}$$

where CRB_1 is the absolute CRB for angle estimation and CRB_2 is the relative CRB for mutual coupling coefficients.

C. Computational Complexity Analysis

In this section, the computational complexity of the proposed Algorithm 1 is provided. The tensor-based 2-D DOA estimation algorithm primarily consists of two main steps, i.e., computing the factor matrices in Step 4 and extracting the DOA information in Step 5. In Step 4, the estimation of factor matrices includes the computation of the SVD of $\mathbf{Y}_S$ and the EVD of $\mathbf{U}_1^{\dagger}\mathbf{U}_2$, whose complexities are $\mathcal{O}((K_2\widetilde{N}_x)^2ML_2)$ and $\mathcal{O}(3K^2K_2\widetilde{N}_x + 2K^2)$, respectively. In addition, $\mathcal{O}(\widetilde{N}_x^2KK_2 + \widetilde{N}_xK)$ algebraic operations is conducted to solve for $\hat{\mathbf{A}}^{(1)}$, by $\hat{\mathbf{a}}_k^{(1)} = (\hat{\mathbf{a}}_k^{(K_2,2)H} \otimes \mathbf{I}_{\widetilde{N}_x})\mathbf{U}_s\mathbf{m}_k$. In Step 5, the calculation of $\{\hat{u}_k\}_{k=1}^K$ and $\{\hat{v}_k\}_{k=1}^K$ requires the complexity of $\mathcal{O}(((\widetilde{N}_y-1)^3 + (\widetilde{N}_x-1)^3)K)$. Therefore, the overall computational complexity can be approximated as $\mathcal{O}((K_2\widetilde{N}_x)^2ML_2 + 3K^2K_2\widetilde{N}_x + 2K^2 + \widetilde{N}_x^2KK_2 + \widetilde{N}_xK + ((\widetilde{N}_y-1)^3 + (\widetilde{N}_x-1)^3)K)$.

V. Simulation Results

In this section, simulation results are provided to verify the effectiveness of the proposed method to estimate azimuth and elevation simultaneously in the presence of unknown mutual coupling. We deploy UPAs with $N_x = N_y = 10$, where the distance between adjacent antennas is set to $d_x = d_y = \lambda/2$. To ensure that the phase difference of signals received by adjacent antennas remains within an appropriate range and avoids causing ambiguity, the antenna spacing should not exceed half a wavelength. In addition, when the antennas are arranged too closely, the mutual coupling effect can severely interfere with the solution of the results [44]. Unless otherwise specified, the coupling coefficients are set as $\tilde{\mathbf{c}} = [1, 0.3527+0.4854j, 0.3527+0.4854j, 0.0927-0.2853j]^{\mathrm{T}}$, i.e., $M_x = M_y = 1$, where the signal-to-noise ratio (SNR) is set to 20 dB and $T = 100$. To further evaluate the performance of the algorithm proposed in this article, we use the root mean square error (RMSE) to describe the estimation performance

$$\mathrm{RMSE} = \sqrt{\frac{1}{LK}\sum_{l=1}^{L}\sum_{k=1}^{K}\left\|\boldsymbol{\Theta}_k - \hat{\boldsymbol{\Theta}}_{lk}\right\|_2^2} \tag{61}$$

where L denotes the number of Monte Carlo trials and is set to 200 in our simulations. Moreover, the vectors $\boldsymbol{\Theta}_k = (\theta_k, \phi_k)$ and $\hat{\boldsymbol{\Theta}}_{lk} = (\hat{\theta}_{lk}, \hat{\phi}_{lk})$ are employed to denote the 2-D DOA of the incident signal and its estimation result in the lth trial, respectively. In the following simulations, our proposed tensor-based algorithm exploiting the Vandermonde structure of factor matrix $\mathbf{A}^{(2)}$ is referred to as Proposed Van-CPD. In our simulations, we consider the following baseline scheme.

1) *2-D MUSIC:* By leveraging the orthogonality between the signal subspace and the noise subspace, the true angle values are obtained using the spectral peak search method [28].
2) *Conventional CPD:* There is no calibration of the effects caused by mutual coupling. Moreover, decompose the signal tensor through the ALS method [30].
3) *Proposed ALS-CPD:* Calibrate the mutual coupling effects by the block transformation matrix $\mathbf{T}$, and obtain factor matrices with the iteration-based ALS.

To validate the source identifiability of the proposed tensor-based DOA estimation algorithm, we present the result of 2-D DOA estimation for $K = 8$ sources under different circumstances in Fig. 3. The azimuth angles of the eight sources are uniformly distributed in $[40°, 320°]$, while their elevation angles are uniformly distributed in $[10°, 80°]$. From Fig. 3(a), we observe that mutual coupling does lead to the performance degradation. It is clear in Fig. 3(b) that our proposed calibration scheme can accurately identify the incident signals.

The result of underdetermined 2-D DOA estimation for $K = 50$ targets using different tensor-based methods is presented in Fig. 4, as a validation for the enhanced source identifiability of the Vandermonde structure-based method, where the parameter $K_2 = 8$. The azimuth angles of the 50 targets are uniformly distributed in $[20°, 320°]$, while their elevation angles are uniformly distributed in $[10°, 82°]$. In this simulation, the number of noise-free snapshots is 100, which is aimed at providing an ideal modeling for the mutual coupling-effected UPA. It is clear in Fig. 4(a) that the ALS decomposition approach for tensor fails to estimate these 50 sources because of the limited source identifiability as claimed in Lemma 3. In contrast, by utilizing the Vandermonde structure, the proposed method is capable of locating all the 50 sources as shown in Fig. 4(b). This result verifies the effectiveness of the proposed algorithm in estimating more sources, which is guaranteed by Lemma 4.

Two closely spaced sources from directions (θ_1, ϕ_1) and (θ_2, ϕ_2) are considered, where $\theta_1 = 30°$ and $\phi_1 = 50°$. In Fig. 5, θ_2 has an angular spacing of δ_θ with θ_1 whereas ϕ_2 remains the same as ϕ_1, i.e., $(\theta_2, \phi_2) = (\theta_1 + \delta_\theta, \phi_1)$. In Fig. 6, ϕ_2 has an angular spacing of δ_ϕ with ϕ_1 whereas θ_2 remains the same as θ_1, i.e., $(\theta_2, \phi_2) = (\theta_1, \phi_1 + \delta_\phi)$. The evaluated methods are identified to successfully distinguish the two sources if $|\hat{\theta}_{lk} - \theta_k| < \delta_\theta/2, |\hat{\phi}_{lk} - \phi_k| < \delta_\theta/2, \forall k = 1, 2$, in Fig. 5, and if $|\hat{\theta}_{lk} - \theta_k| < \delta_\phi/2, |\hat{\phi}_{lk} - \phi_k| < \delta_\phi/2, \forall k = 1, 2$, in Fig. 6 for each trial. The probability of successful resolution (PSR) can then be calculated as the percentage of successful trials [52]. In this and the following simulations, K_2 is set to 6. The proposed tensor-based algorithms present a greater angular resolution than MUSIC. This is because the accuracy of the MUSIC algorithm heavily relies on the grid density of the spectral peak search. In our trials, the search density for each dimension is set to 0.5°, which is insufficient to effectively distinguish and detect targets with extremely small spacing. In contrast, the

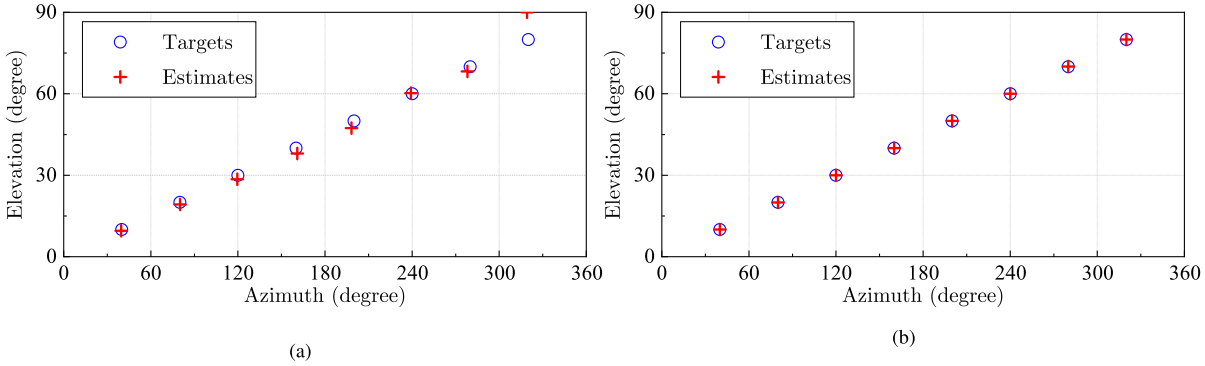

Fig. 3. Source identifiability of the proposed calibration scheme with eight sources under different circumstances. (a) Without calibration. (b) With calibration.

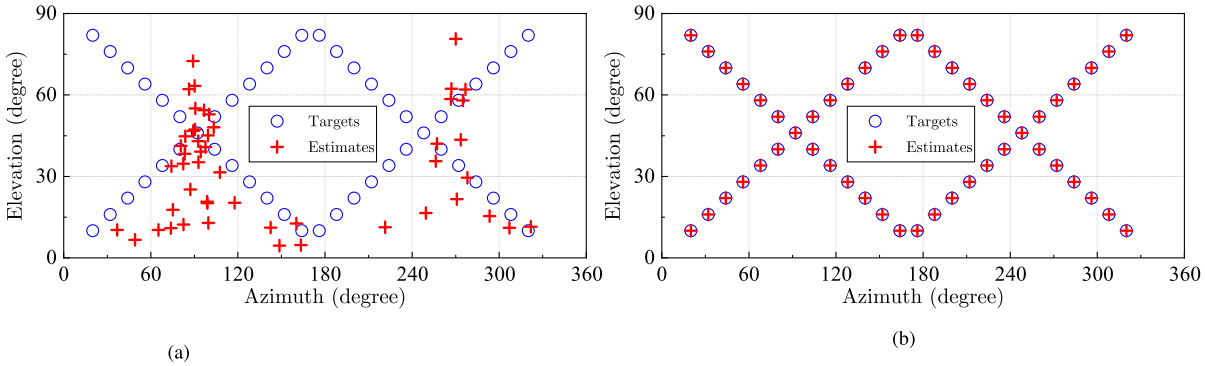

Fig. 4. Comparison of source identifiability between two tensor-based algorithms with 50 targets. (a) Proposed ALS-CPD. (b) Proposed Van-CPD.

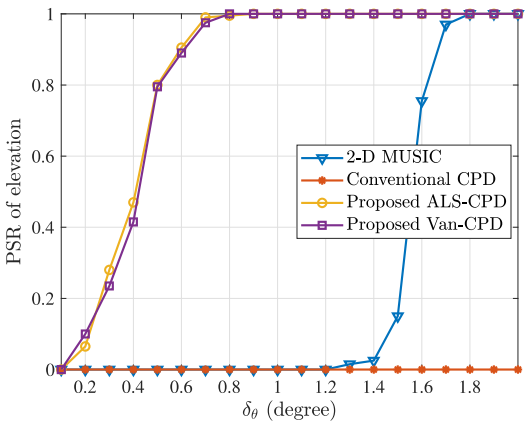

Fig. 5. PSR versus δ_θ.

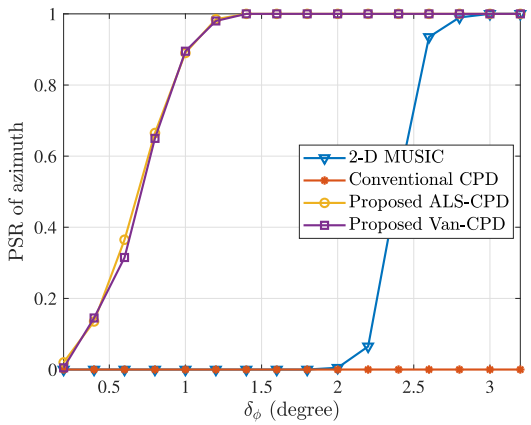

Fig. 6. PSR versus δ_ϕ.

algorithm based on tensor decomposition can estimate angles in a gridless manner.

Figs. 7 and 8 depict the results of the 2-D DOA estimation in terms of success rate and CPU runtime, where SNR is set to 20 dB. A target is considered successfully estimated if the 2-D DOA estimation error satisfies $\|\boldsymbol{\Theta}_k - \hat{\boldsymbol{\Theta}}_{lk}\|_2 \leq 2^\circ$. Only if all the K targets are successfully estimated, this trial is seen as a successful one. The value of the overall success rate is the average taken over all Monte Carlo trials. From Fig. 7, it can be observed that the success rate of the MUSIC method decreases to zero when the number of targets exceeds 11. But the performance of the tensor-based method can be much better. Meanwhile, we can also observe that due to the presence of the noise term $\mathcal{N}$ in (19), the uniqueness conditions for tensor decomposition are violated, and the number of targets that can be estimated is consequently reduced. Nevertheless, as we can see from Fig. 8, when the number of targets increases, the method that fully leverages the Vandermonde structural properties of the factor matrices exhibits a significant advantage in terms of runtime. This is because, for the MUSIC algorithm, the complexity of its spectral peak search is extremely highly dependent on the density of the discretized grid, but does not change significantly with an increase in the number of targets. In the case of the ALS-based algorithm, the computational cost is predominantly governed by the number of iterations. As the number of targets grows, the ALS-based algorithm often experiences convergence challenges, necessitating more iterations and thus driving a sharp increase in computational load.

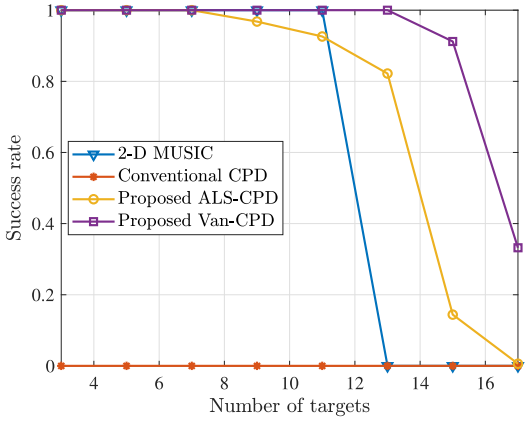

Fig. 7. Success rate versus the number of targets.

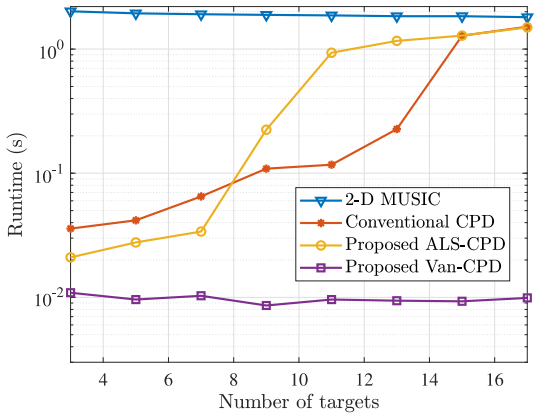

Fig. 8. CPU runtime versus the number of targets.

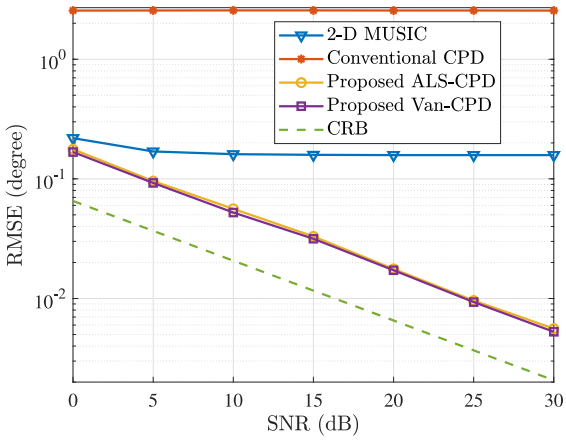

Fig. 9. RMSE versus SNR.

To shed light on the performance of the proposed tensor-based algorithm, we further investigate the RMSE of 2-D DOA estimation with other algorithms. Fig. 9 depicts the RMSE versus SNR, where the number of snapshots is fixed to 100 with SNR varying among $[0, 5, 10, 15, 20, 25, 30]$ dB. Similarly, we investigate the situations where SNR is set to 20 dB, and $T = 5, 10, 50, 100, 150, 200, 250, 300$ in Fig. 10. The true directions of the targets are $(30°, 40.1°)$ and $(58°, 45.7°)$. It can be observed that 2-D MUSIC encounters performance bottlenecks due to limited grid density. In contrast, the performance of our proposed tensor-based algorithms continuously improves

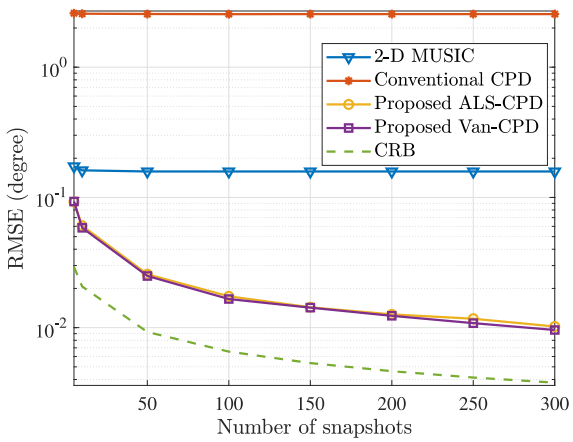

Fig. 10. RMSE versus the number of snapshots.

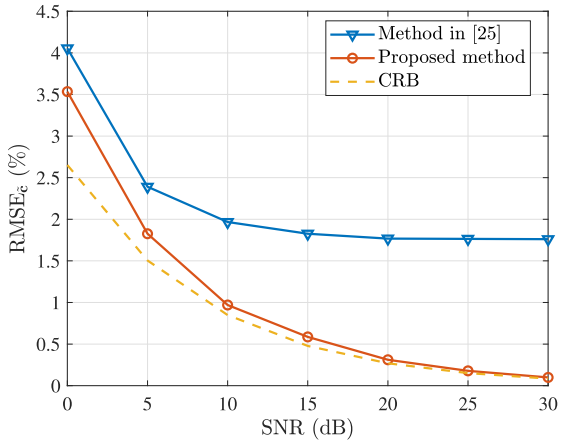

Fig. 11. RMSE$_{\tilde{\mathbf{c}}}$ versus SNR.

with increasing SNR and number of snapshots. This is because tensor decomposition fully utilizes the information of each factor matrix, enabling high-precision estimation. Meanwhile, the algebraic operation-based solution method leveraging the Vandermonde structure of factor matrices significantly reduces computational complexity while slightly improving the accuracy of angle estimation.

In order to better investigate the estimation performance of mutual coupling coefficients, two incident sources are configured in this simulation, which maintain consistency with $(30°, 40.1°)$ and $(58°, 45.7°)$. We define RMSE$_{\tilde{\mathbf{c}}}$ to quantization estimation error of mutual coupling coefficients as follows:

$$\text{RMSE}_{\tilde{\mathbf{c}}} = \sqrt{\frac{1}{L}\sum_{l=1}^{L}\frac{\left\|\hat{\tilde{\mathbf{c}}}_l - \tilde{\mathbf{c}}\right\|_2^2}{\|\tilde{\mathbf{c}}\|_2^2}} \times 100\% \tag{62}$$

where $\hat{\tilde{\mathbf{c}}}_l$ denotes the estimated value of $\tilde{\mathbf{c}}_l$ in the lth trial.

Figs. 11 and 12 present the estimation errors of mutual coupling coefficient vector $\tilde{\mathbf{c}}$ versus input SNR and the number of snapshots. It is observed that the estimation of coupling coefficients is very effective, and the proposed algorithm generates very low RMSE when the SNR is higher than 5 dB. Furthermore, as the SNR and T increase, the error in the estimation results approaches the CRB. Compared to the

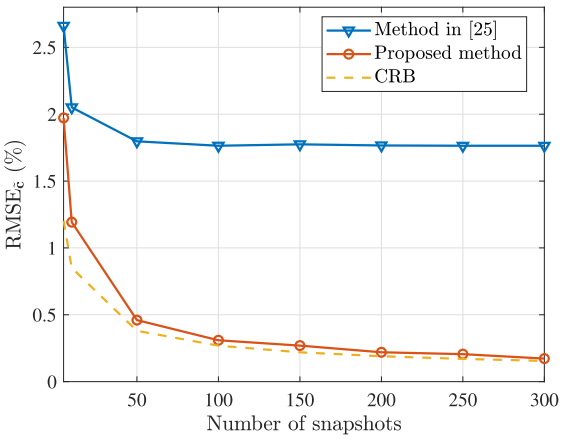

Fig. 12. RMSE$_{\tilde{\mathbf{c}}}$ versus the number of snapshots.

auxiliary array element method proposed in [28], the algorithm introduced in this article achieves significantly smaller RMSE. This advantage becomes particularly evident under harsh conditions, such as low SNR and limited snapshots. The primary reason lies in the fact that the auxiliary array element method employs least-squares estimation for mutual coupling coefficients. However, least-squares estimation inherently suffers from degraded accuracy when SNR is low or the number of snapshots is insufficient.

VI. Conclusion

In this article, we proposed a tensor-based 2-D DOA estimation method for UPAs under unknown mutual coupling effects. We constructed a calibration matrix to eliminate mutual coupling effects by exploiting the inherent structure of MCM. The received signals were then reformulated into a tensor model admitting canonical polyadic decomposition, where factor matrices explicitly incorporate the azimuth and elevation angles of arrival. Given the Vandermonde structure of these factor matrices in our model, we optimized the solving procedure by proposing an algebraic-based factor matrices estimation method without the necessity of iteration. This enabled direct extraction of 2-D DOA parameters from the factor matrices. Subsequently, closed-form solutions for mutual coupling coefficients were derived from the estimated angles. We further established theoretical guarantees, including uniqueness conditions for tensor decomposition, as well as CRB of joint 2-D DOA and MCM estimation under the circumstance of the UPAs. We further provided the computational complexity analysis of our method. From the simulation results, we demonstrated the superiority of the proposed tensor-based algorithm over state-of-the-art methods in terms of computational complexity, resolution, and estimation accuracy.

Appendix A
Proof for Lemma 1

For the sake of convenience in expression, let us first consider the calculation result for an arbitrary single signal source, which can be subsequently extended to multiple sources. To be specific, for the kth signal source, we have

$$\mathbf{TCa}\left(\theta_k,\phi_k\right)=\begin{bmatrix}\sum\limits_{m_y=-M_y}^{M_y}\widetilde{\mathbf{TC}}_{|m_y|}\beta_k^{M_y+m_y}\mathbf{a}_x\\ \sum\limits_{m_y=-M_y}^{M_y}\widetilde{\mathbf{TC}}_{|m_y|}\beta_k^{M_y+m_y+1}\mathbf{a}_x\\ \vdots\\ \sum\limits_{m_y=-M_y}^{M_y}\widetilde{\mathbf{TC}}_{|m_y|}\beta_k^{M_y+m_y+\widetilde{N}_y-1}\mathbf{a}_x\end{bmatrix} \tag{63}$$

where $\mathbf{a}_x \triangleq \mathbf{a}_x(\theta_k,\phi_k)$ and the equality follows from the definition of $\mathbf{C}$ in (9). Take the first element of (63) as an example, we can obtain

$$\begin{aligned}&\sum_{m_y=-M_y}^{M_y}\widetilde{\mathbf{TC}}_{|m_y|}\beta_k^{M_y+m_y}\mathbf{a}_x\\ &=\sum_{m_y=-M_y}^{M_y}\sum_{m_x=-M_x}^{M_x}c_{|m_y|,|m_x|}\alpha_k^{m_x}\beta_k^{m_y}\begin{bmatrix}\alpha_k^{M_x}\beta_k^{M_y}\\ \alpha_k^{M_x+1}\beta_k^{M_y}\\ \vdots\\ \alpha_k^{M_x+\widetilde{N}_x-1}\beta_k^{M_y}\end{bmatrix}\end{aligned} \tag{64}$$

where $k=1,2,\ldots,K$. The equality holds by exploiting the definition of $\mathbf{a}_x$ and the submatrix $\mathbf{C}_{|m_y|}$ of $\mathbf{C}$. According to the key observation that block transformation matrix $\mathbf{T}$ plays a role of selecting rows from steering vectors, the calculation result of (63) is

$$\mathbf{TCa}\left(\theta_k,\phi_k\right)=g_k\mathbf{Ta}\left(\theta_k,\phi_k\right) \tag{65}$$

where $g_k=\sum_{m_x=-M_x}^{M_x}\sum_{m_y=-M_y}^{M_y}c_{|m_y|,|m_x|}\alpha_k^{m_x}\beta_k^{m_y}$.

Appendix B
Details of FIM

Inspired by (55)–(58), we can obtain the expressions as follows:

$$\begin{aligned}\mathbf{F}_{\boldsymbol{\theta}\boldsymbol{\phi}}=2T\mathcal{R}\Big\{&\left(\mathbf{R}_s\bar{\mathbf{A}}^H\mathbf{R}_c^{-1}\dot{\bar{\mathbf{A}}}_{\boldsymbol{\phi}}\right)\circledast\left(\mathbf{R}_s\bar{\mathbf{A}}^H\mathbf{R}_c^{-1}\dot{\bar{\mathbf{A}}}_{\boldsymbol{\theta}}\right)^{\mathrm{T}}\\&+\left(\mathbf{R}_s\bar{\mathbf{A}}^H\mathbf{R}_c^{-1}\bar{\mathbf{A}}\mathbf{R}_s\right)\circledast\left(\dot{\bar{\mathbf{A}}}_{\boldsymbol{\phi}}^H\mathbf{R}_c^{-1}\dot{\bar{\mathbf{A}}}_{\boldsymbol{\theta}}\right)^{\mathrm{T}}\Big\}\end{aligned} \tag{66}$$

$$\begin{aligned}F_{\bar{\xi}_i\bar{\xi}_j}=2T\mathcal{R}\Big\{&\mathrm{tr}\left\{\mathbf{R}_c^{-1}\dot{\bar{\mathbf{A}}}_{\bar{\xi}_i}\mathbf{R}_s\bar{\mathbf{A}}^H\mathbf{R}_c^{-1}\dot{\bar{\mathbf{A}}}_{\bar{\xi}_i}\mathbf{R}_s\bar{\mathbf{A}}^H\right\}\\&+\mathrm{tr}\left\{\mathbf{R}_c^{-1}\dot{\bar{\mathbf{A}}}_{\bar{\xi}_i}\mathbf{R}_s\bar{\mathbf{A}}^H\mathbf{R}_c^{-1}\bar{\mathbf{A}}\mathbf{R}_s\dot{\bar{\mathbf{A}}}_{\bar{\xi}_i}^H\right\}\Big\}\end{aligned} \tag{67}$$

$$\begin{aligned}\mathbf{f}_{\boldsymbol{\theta}\bar{\xi}_j}=2T\mathcal{R}\Big\{&\mathrm{diag}\left\{\mathbf{R}_s\bar{\mathbf{A}}^H\mathbf{R}_c^{-1}\dot{\bar{\mathbf{A}}}_{\bar{\xi}_j}\mathbf{R}_s\bar{\mathbf{R}}^H\mathbf{R}_c^{-1}\dot{\bar{\mathbf{A}}}_{\boldsymbol{\theta}}\right\}\\&+\mathrm{diag}\left\{\mathbf{R}_s\bar{\mathbf{A}}^H\mathbf{R}_c^{-1}\bar{\mathbf{A}}\mathbf{R}_s\dot{\bar{\mathbf{A}}}_{\bar{\xi}_j}^H\mathbf{R}_c^{-1}\dot{\bar{\mathbf{A}}}_{\boldsymbol{\theta}}\right\}\Big\}\end{aligned} \tag{68}$$

$$\begin{aligned}\mathbf{F}_{\boldsymbol{\phi}\boldsymbol{\theta}}=2T\mathcal{R}\Big\{&\left(\mathbf{R}_s\bar{\mathbf{A}}^H\mathbf{R}_c^{-1}\dot{\bar{\mathbf{A}}}_{\boldsymbol{\theta}}\right)\circledast\left(\mathbf{R}_s\bar{\mathbf{A}}^H\mathbf{R}_c^{-1}\dot{\bar{\mathbf{A}}}_{\boldsymbol{\phi}}\right)^{\mathrm{T}}\\&+\left(\mathbf{R}_s\bar{\mathbf{A}}^H\mathbf{R}_c^{-1}\bar{\mathbf{A}}\mathbf{R}_s\right)\circledast\left(\dot{\bar{\mathbf{A}}}_{\boldsymbol{\theta}}^H\mathbf{R}_c^{-1}\dot{\bar{\mathbf{A}}}_{\boldsymbol{\phi}}\right)^{\mathrm{T}}\Big\}\end{aligned} \tag{69}$$

$$\begin{aligned}\mathbf{f}_{\boldsymbol{\theta}\bar{\xi}_j}=2T\mathcal{R}\Big\{&\mathrm{diag}\left\{\mathbf{R}_s\bar{\mathbf{A}}^H\mathbf{R}_c^{-1}\dot{\bar{\mathbf{A}}}_{\bar{\xi}_j}\mathbf{R}_s\mathbf{R}_c^H\mathbf{R}_c^{-1}\dot{\bar{\mathbf{A}}}_{\boldsymbol{\theta}}\right\}\\&+\mathrm{diag}\left\{\mathbf{R}_s\bar{\mathbf{A}}^H\mathbf{R}_c^{-1}\bar{\mathbf{A}}\mathbf{R}_s\dot{\bar{\mathbf{A}}}_{\bar{\xi}_j}^H\mathbf{R}_c^{-1}\dot{\bar{\mathbf{A}}}_{\boldsymbol{\theta}}\right\}\Big\}\end{aligned} \tag{70}$$

$$\mathbf{f}_{\boldsymbol{\phi}\bar{\xi}_j} = 2\mathcal{TR}\left\{\text{diag}\left\{\mathbf{R}_s\bar{\mathbf{A}}^H\mathbf{R}_c^{-1}\dot{\bar{\mathbf{A}}}_{\bar{\xi}_j}\mathbf{R}_s\mathbf{R}_c^H\mathbf{R}_c^{-1}\dot{\mathbf{A}}_{\boldsymbol{\phi}}\right\} + \text{diag}\left\{\mathbf{R}_s\bar{\mathbf{A}}^H\mathbf{R}_c^{-1}\bar{\mathbf{A}}\mathbf{R}_s\dot{\bar{\mathbf{A}}}_{\bar{\xi}_j}^H\mathbf{R}_c^{-1}\dot{\mathbf{A}}_{\boldsymbol{\phi}}\right\}\right\} \tag{71}$$

$$\mathbf{f}_{\boldsymbol{\phi}\tilde{\xi}_j} = 2\mathcal{TR}\left\{\text{diag}\left\{\mathbf{R}_s\bar{\mathbf{A}}^H\mathbf{R}_c^{-1}\dot{\bar{\mathbf{A}}}_{\tilde{\xi}_j}\mathbf{R}_s\mathbf{R}_c^H\mathbf{R}_c^{-1}\dot{\mathbf{A}}_{\boldsymbol{\phi}}\right\} + \text{diag}\left\{\mathbf{R}_s\bar{\mathbf{A}}^H\mathbf{R}_c^{-1}\bar{\mathbf{A}}\mathbf{R}_s\dot{\bar{\mathbf{A}}}_{\tilde{\xi}_j}^H\mathbf{R}_c^{-1}\dot{\mathbf{A}}_{\boldsymbol{\phi}}\right\}\right\} \tag{72}$$

$$F_{\tilde{\xi}_i\tilde{\xi}_j} = 2\mathcal{TR}\left\{\text{tr}\left\{\mathbf{R}_c^{-1}\dot{\bar{\mathbf{A}}}_{\tilde{\xi}_i}\mathbf{R}_s\bar{\mathbf{A}}^H\mathbf{R}_c^{-1}\dot{\bar{\mathbf{A}}}_{\tilde{\xi}_i}\mathbf{R}_s\bar{\mathbf{A}}^H\right\} + \text{tr}\left\{\mathbf{R}_c^{-1}\dot{\bar{\mathbf{A}}}_{\tilde{\xi}_i}\mathbf{R}_s\bar{\mathbf{A}}^H\mathbf{R}_c^{-1}\bar{\mathbf{A}}\mathbf{R}_s\dot{\bar{\mathbf{A}}}_{\tilde{\xi}_i}^H\right\}\right\} \tag{73}$$

where $\dot{\bar{\mathbf{A}}}_{\bar{\xi}_i} = (\partial\mathbf{C})/(\partial\bar{\xi}_i)\mathbf{A}$ and $\dot{\bar{\mathbf{A}}}_{\tilde{\xi}_i} = (\partial\mathbf{C})/(\partial\tilde{\xi}_i)\mathbf{A}$, $i, j = 1, 2, \ldots, M$. Accordingly, the FIM can be obtained.

REFERENCES

[1] H. Krim and M. Viberg, "Two decades of array signal processing research: The parametric approach," *IEEE Signal Process. Mag.*, vol. 13, no. 4, pp. 67–94, Jul. 1996.

[2] X. Luo, Q. Lin, R. Zhang, H.-H. Chen, X. Wang, and M. Huang, "ISAC—A survey on its layered architecture, technologies, standardizations, prototypes and testbeds," *IEEE Commun. Surveys Tuts.*, early access, Apr. 29, 2025, doi: 10.1109/COMST.2025.3565534.

[3] R. Zhang, B. Shim, and W. Wu, "Direction-of-arrival estimation for large antenna arrays with hybrid analog and digital architectures," *IEEE Trans. Signal Process.*, vol. 70, pp. 72–88, 2022.

[4] F. Wen, Z. Zhang, H. Sun, G. Gui, H. Sari, and F. Adachi, "2D-DOA estimation auxiliary localization of anonymous UAV using EMVS-MIMO radar," *IEEE Internet Things J.*, vol. 11, no. 9, pp. 16255–16266, May 2024.

[5] X. Mestre and M. Á. Lagunas, "Modified subspace algorithms for DoA estimation with large arrays," *IEEE Trans. Signal Process.*, vol. 56, no. 2, pp. 598–614, Feb. 2008.

[6] L. Cheng, Y.-C. Wu, J. Zhang, and L. Liu, "Subspace identification for DOA estimation in massive/full-dimension MIMO systems: Bad data mitigation and automatic source enumeration," *IEEE Trans. Signal Process.*, vol. 63, no. 22, pp. 5897–5909, Nov. 15, 2015.

[7] R. Zhang, W. Wu, X. Chen, Z. Gao, and Y. Cai, "Terahertz integrated sensing and communication-empowered UAVs in 6G: A transceiver design perspective," *IEEE Veh. Technol. Mag.*, early access, Feb. 17, 2025, doi: 10.1109/MVT.2025.3531088.

[8] R. Zhang, B. Shim, and H. Zhao, "Downlink compressive channel estimation with phase noise in massive MIMO systems," *IEEE Trans. Commun.*, vol. 68, no. 9, pp. 5534–5548, Sep. 2020.

[9] H. Zhao, Z. Ding, Q. Wang, W. Xia, B. Xu, and H. Zhu, "Antenna selection method for distributed dual-function radar communication in MIMO system," *Chin. J. Electron.*, vol. 34, no. 1, pp. 1–11, Jan. 2025.

[10] A. Chen, W. Xu, Y. Wang, Y. Huang, and G. Gui, "Deep-unrolling-based gridless channel estimation in massive SIMO systems with antenna failures," *IEEE Wireless Commun. Lett.*, vol. 14, no. 3, pp. 766–770, Mar. 2025.

[11] D. Xia et al., "Accurate 2-D DoA estimation based on active metasurface with nonuniformly periodic time modulation," *IEEE Trans. Microw. Theory Techn.*, vol. 71, no. 8, pp. 3424–3435, Aug. 2023.

[12] G. Chen, R. Zhang, H. Zhang, C. Miao, Y. Ma, and W. Wu, "Energy-efficient beamforming for downlink multi-user systems with dynamic metasurface antennas," *IEEE Commun. Lett.*, vol. 29, no. 2, pp. 284–288, Feb. 2025.

[13] L. Yao, R. Zhang, C. Hu, and W. Wu, "Off-grid DOA estimation for metasurface antenna systems using sparse Bayesian learning," *AEU-Int. J. Electron. Commun.*, vol. 190, Mar. 2025, Art. no. 155615.

[14] R. Schmidt, "Multiple emitter location and signal parameter estimation," *IEEE Trans. Antennas Propag.*, vol. AP-34, no. 3, pp. 276–280, Mar. 1986.

[15] R. Roy and T. Kailath, "ESPRIT-estimation of signal parameters via rotational invariance techniques," *IEEE Trans. Acoust. Speech Signal Process.*, vol. 37, no. 7, pp. 984–995, Jul. 1989.

[16] R. Rubinstein, M. Zibulevsky, and M. Elad, "Double sparsity: Learning sparse dictionaries for sparse signal approximation," *IEEE Trans. Signal Process.*, vol. 58, no. 3, pp. 1553–1564, Mar. 2010.

[17] S. Li and B. Yang, "A new pan-sharpening method using a compressed sensing technique," *IEEE Trans. Geosci. Remote Sens.*, vol. 49, no. 2, pp. 738–746, Feb. 2011.

[18] D. Malioutov, M. Cetin, and A. S. Willsky, "A sparse signal reconstruction perspective for source localization with sensor arrays," *IEEE Trans. Signal Process.*, vol. 53, no. 8, pp. 3010–3022, Aug. 2005.

[19] S. G. Mallat and Z. Zhang, "Matching pursuits with time-frequency dictionaries," *IEEE Trans. Signal Process.*, vol. 41, no. 12, pp. 3397–3415, Dec. 1993.

[20] Z. Yang, L. Xie, and C. Zhang, "Off-grid direction of arrival estimation using sparse Bayesian inference," *IEEE Trans. Signal Process.*, vol. 61, no. 1, pp. 38–43, Jan. 1, 2013.

[21] F. Wen, J. Shi, G. Gui, C. Yuen, H. Sari, and F. Adachi, "Joint DOD and DOA estimation for NLOS target using IRS-aided bistatic MIMO radar," *IEEE Trans. Veh. Technol.*, vol. 73, no. 10, pp. 15798–15802, Oct. 2024.

[22] C.-L. Liu and P. P. Vaidyanathan, "Super nested arrays: Linear sparse arrays with reduced mutual coupling—Part I: Fundamentals," *IEEE Trans. Signal Process.*, vol. 64, no. 15, pp. 3997–4012, Aug. 2016.

[23] P. Pal and P. P. Vaidyanathan, "Nested arrays: A novel approach to array processing with enhanced degrees of freedom," *IEEE Trans. Signal Process.*, vol. 58, no. 8, pp. 4167–4181, Aug. 2010.

[24] P. P. Vaidyanathan and P. Pal, "Sparse sensing with co-prime samplers and arrays," *IEEE Trans. Signal Process.*, vol. 59, no. 2, pp. 573–586, Feb. 2011.

[25] B. Friedlander and A. J. Weiss, "Direction finding in the presence of mutual coupling," *IEEE Trans. Antennas Propag.*, vol. 39, no. 3, pp. 273–284, Mar. 1991.

[26] P. Chen, Z. Cao, Z. Chen, and X. Wang, "Off-grid DOA estimation using sparse Bayesian learning in MIMO radar with unknown mutual coupling," *IEEE Trans. Signal Process.*, vol. 67, no. 1, pp. 208–220, Jan. 2019.

[27] Y. Yu and H. T. Hui, "Design of a mutual coupling compensation network for a small receiving monopole array," *IEEE Trans. Microw. Theory Techn.*, vol. 59, no. 9, pp. 2241–2245, Sep. 2011.

[28] Z. Ye and C. Liu, "2-D DOA estimation in the presence of mutual coupling," *IEEE Trans. Antennas Propag.*, vol. 56, no. 10, pp. 3150–3158, Oct. 2008.

[29] R. Goossens and H. Rogier, "A hybrid UCA-RARE/root-MUSIC approach for 2-D direction of arrival estimation in uniform circular arrays in the presence of mutual coupling," *IEEE Trans. Antennas Propag.*, vol. 55, no. 3, pp. 841–849, Mar. 2007.

[30] J. Salmi, A. Richter, and V. Koivunen, "Sequential unfolding SVD for tensors with applications in array signal processing," *IEEE Trans. Signal Process.*, vol. 57, no. 12, pp. 4719–4733, Dec. 2009.

[31] N. D. Sidiropoulos, L. De Lathauwer, X. Fu, K. Huang, E. E. Papalexakis, and C. Faloutsos, "Tensor decomposition for signal processing and machine learning," *IEEE Trans. Signal Process.*, vol. 65, no. 13, pp. 3551–3582, Jul. 2017.

[32] D. Nion and N. D. Sidiropoulos, "Tensor algebra and multidimensional harmonic retrieval in signal processing for MIMO radar," *IEEE Trans. Signal Process.*, vol. 58, no. 11, pp. 5693–5705, Nov. 2010.

[33] H. Chen, F. Ahmad, S. Vorobyov, and F. Porikli, "Tensor decompositions in wireless communications and MIMO radar," *IEEE J. Sel. Topics Signal Process.*, vol. 15, no. 3, pp. 438–453, Apr. 2021.

[34] R. Zhang, L. Cheng, S. Wang, Y. Lou, W. Wu, and D. W. K. Ng, "Tensor decomposition-based channel estimation for hybrid mmWave massive MIMO in high-mobility scenarios," *IEEE Trans. Commun.*, vol. 70, no. 9, pp. 6325–6340, Sep. 2022.

[35] W. Wang, X. Wang, Y. Guo, and G. Gui, "Parameter estimation with bistatic MIMO radar: A coarray tensor decomposition framework," *IEEE Trans. Aerosp. Electron. Syst.*, vol. 61, no. 2, pp. 4450–4465, Apr. 2025.

[36] Q. Xie, Z. Wang, F. Wen, J. He, and T.-K. Truong, "Coarray tensor train decomposition for bistatic MIMO radar with uniform planar array," *IEEE Trans. Antennas Propag.*, vol. 73, no. 8, pp. 5310–5323, Aug. 2025.

[37] Q. Xie, F. Wen, X. Xie, Z. Wang, and X. Pan, "Coarray tensor train aided target localization for bistatic MIMO radar," *IEEE Signal Process. Lett.*, vol. 32, pp. 46–50, 2024.

[38] Q. Xie, J. Shi, F. Wen, and Z. Zheng, "Higher-order tensor decomposition for 2D-DOD and 2D-DOA estimation in bistatic MIMO radar," *Signal Process.*, vol. 238, Jan. 2026, Art. no. 110196.

[39] R. Zhang et al., "Integrated sensing and communication with massive MIMO: A unified tensor approach for channel and target parameter estimation," *IEEE Trans. Wireless Commun.*, vol. 23, no. 8, pp. 8571–8587, Aug. 2024.

[40] R. Zhang et al., "Channel estimation for movable-antenna MIMO systems via tensor decomposition," *IEEE Wireless Commun. Lett.*, vol. 13, no. 11, pp. 3089–3093, Nov. 2024, doi: 10.1109/LWC.2024.3450592.

[41] X. Lan, L. Wang, Y. Wang, C. Choi, and D. Choi, "Tensor 2-D DOA estimation for a cylindrical conformal antenna array in a massive MIMO system under unknown mutual coupling," *IEEE Access*, vol. 6, pp. 7864–7871, 2018.
[42] F. Xu, H. Zheng, and S. A. Vorobyov, "Tensor-based 2-D DOA estimation for L-shaped nested array," *IEEE Trans. Aerosp. Electron. Syst.*, vol. 60, no. 1, pp. 604–618, Feb. 2024.
[43] M. Fu, Z. Zheng, W.-Q. Wang, and H. C. So, "Virtual array interpolation for 2-D DOA and polarization estimation using coprime EMVS array via tensor nuclear norm minimization," *IEEE Trans. Signal Process.*, vol. 71, pp. 3637–3650, 2023.
[44] S. Lou, S. Qian, S. Lian, W. Wang, H. Bao, and G. Leng, "Analysis of high-order mutual coupling effect of antenna arrays based on infinitesimal dipole model," *IEEE Trans. Antennas Propag.*, vol. 73, no. 6, pp. 3628–3638, Jun. 2025.
[45] A. Stegeman and N. D. Sidiropoulos, "On Kruskal's uniqueness condition for the candecomp/parafac decomposition," *Linear Algebra Appl.*, vol. 420, nos. 2–3, pp. 540–552, Jan. 2007.
[46] C. M. S. See and A. B. Gershman, "Direction-of-arrival estimation in partly calibrated subarray-based sensor arrays," *IEEE Trans. Signal Process.*, vol. 52, no. 2, pp. 329–338, Feb. 2004.
[47] F. Wen, J. Wang, J. Shi, and G. Gui, "Auxiliary vehicle positioning based on robust DOA estimation with unknown mutual coupling," *IEEE Internet Things J.*, vol. 7, no. 6, pp. 5521–5532, Jun. 2020.
[48] B. Li, W. Bai, and G. Zheng, "Successive ESPRIT algorithm for joint DOA-range-polarization estimation with polarization sensitive FDA-MIMO radar," *IEEE Access*, vol. 6, pp. 36376–36382, 2018.
[49] L. Xu, J. Li, and P. Stoica, "Target detection and parameter estimation for MIMO radar systems," *IEEE Trans. Aerosp. Electron. Syst.*, vol. 44, no. 3, pp. 927–939, Jul. 2008.
[50] R. Zhang et al., "Tensor-based channel estimation for extremely large-scale MIMO-OFDM with dynamic metasurface antennas," *IEEE Trans. Wireless Commun.*, vol. 24, no. 7, pp. 6052–6068, Jul. 2025, doi: 10.1109/TWC.2025.3551144.
[51] M. Sørensen and L. De Lathauwer, "Blind signal separation via tensor decomposition with Vandermonde factor: Canonical polyadic decomposition," *IEEE Trans. Signal Process.*, vol. 61, no. 22, pp. 5507–5519, Nov. 15, 2013.
[52] H. Zheng, C. Zhou, Z. Shi, Y. Gu, and Y. D. Zhang, "Coarray tensor direction-of-arrival estimation," *IEEE Trans. Signal Process.*, vol. 71, pp. 1128–1142, 2023.

Lei Yao was born in Jiangsu, China. He is currently pursuing the B.E. degree in communication engineering with Qian Xuesen College, Nanjing University of Science and Technology (NJUST), Nanjing, China.

He has authored or co-authored several journal articles. His research interests include direction-of-arrival estimation, integrated sensing and communication (ISAC), massive multiple-input multiple-output (MIMO), and affine frequency division multiplexing (AFDM).

Mr. Yao received the National Scholarship for Undergraduates in 2024 and 2025.

Ruoyu Zhang (Senior Member, IEEE) received the B.E. and Ph.D. degrees in information and communication engineering from Harbin Institute of Technology, Harbin, China, in 2014 and 2019, respectively.

From 2017 to 2018, he was a Visiting Student at the Department of Electrical and Computer Engineering, The University of British Columbia, Vancouver, BC, Canada. He is currently an Associate Professor with the School of Electronic and Optical Engineering, Nanjing University of Science and Technology. His research interests include integrated sensing and communication, massive MIMO, millimeter-wave communications, and sparse signal processing.

Changcheng Hu received the B.E. degree in communication engineering from Anhui University, Hefei, China, in 2023. He is currently pursuing the M.S. degree with the School of Electronic and Optical Engineering, Nanjing University of Science and Technology (NJUST), Nanjing, China.

His current research interests include direction-of-arrival estimation and signal processing based on metasurfaces.

Chengzhi Ye (Student Member, IEEE) was born in Yangzhou, Jiangsu, China, in 2005. He is currently pursuing the B.E. degree in communication engineering with Qian Xuesen College, Nanjing University of Science and Technology (NJUST), Nanjing, China.

His research interests include integrated sensing and communication (ISAC), movable antenna (MA), channel estimation, and direction-of-arrival estimation, with a focus on developing robust calibration algorithms to address practical array imperfections, such as gain–phase errors, mutual coupling, and position errors.

Wen Wu (Senior Member, IEEE) received the Ph.D. degree in electromagnetic field and microwave technology from Southeast University, Nanjing, China, in 1997.

He is currently a Professor with the School of Electronic and Optical Engineering, Nanjing University of Science and Technology, where he is also a Director with the Key Laboratory of Near-Range RF Sensing ICs and Microsystems (NJUST), Ministry of Education. He has authored or co-authored over 300 journal articles and conference papers, and has submitted over 30 patent applications. His current research interests include microwave and millimeter-wave theories and technologies, microwave and millimeter-wave detection, and multimodal compound detection.

Dr. Wu was a recipient of the Ministerial and Provincial-Level Science and Technology Award six times.

Byonghyo Shim (Fellow, IEEE) received the B.S. and M.S. degrees in control and instrumentation engineering from Seoul National University, Seoul, South Korea, in 1995 and 1997, respectively, and the M.S. degree in mathematics and the Ph.D. degree in electrical and computer engineering from the University of Illinois at Urbana-Champaign (UIUC), Champaign, IL, USA, in 2004 and 2005, respectively.

From 1997 to 2000, he was an Officer (First Lieutenant) and an Academic Instructor (full-time) with the Department of Electronics Engineering, Korean Air Force Academy, Cheongju, South Korea. From 2005 to 2007, he was a Staff Engineer with Qualcomm Inc., San Diego, CA, USA. From 2007 to 2014, he was an Associate Professor with the School of Information and Communication, Korea University, Seoul. Since 2014, he has been with Seoul National University (SNU), where he is currently a Professor with the Department of Electrical and Computer Engineering and the Vice Dean of Academic Affairs with the Engineering College. His research interests include wireless communications, deep learning, and statistical signal processing.

Dr. Shim was a recipient of the M. E. Van Valkenburg Research Award from the ECE Department, University of Illinois, in 2005; the Haedong Young Engineer Award from IEIE in 2010; the Irwin Jacobs Award from Qualcomm and KICS in 2016; the Shinyang Research Award from the Engineering College of SNU in 2017; the Okawa Foundation Research Award in 2020; the IEEE Comsoc AP Outstanding Paper Award in 2021; and the JCN Best Paper Award in 2024. He has served as an Associate Editor for IEEE TRANSACTIONS ON WIRELESS COMMUNICATIONS, IEEE TRANSACTIONS ON COMMUNICATIONS, IEEE TRANSACTIONS ON VEHICULAR TECHNOLOGY, IEEE TRANSACTIONS ON SIGNAL PROCESSING, IEEE WIRELESS COMMUNICATIONS LETTERS, and *Journal of Communications and Networks* (JCN); and a Guest Editor for IEEE JOURNAL ON SELECTED AREAS IN COMMUNICATIONS.